AGU ADVANCING EARTH AND SPACE SCIENCES

JGR Solid Earth

Key Points:

- First high-precision Cr isotope compositions on a unique suite of meta-serpentinites
- Oceanic serpentinites with significant Cr loss tend to exhibit remarkably higher δ^{53}Cr
- Significant Cr isotope fractionation occurs during prograde dehydration of serpentinites in subduction zones

Supporting Information:

Supporting Information may be found in the online version of this article.

Correspondence to:

Y.-X. Chen and J. Shen,
yxchen07@ustc.edu.cn;
sjlcwqqq@ustc.edu.cn

Chromium Isotope Behavior During Serpentinite Dehydration in Oceanic Subduction Zones

Jia-Wei Xiong[1], Yi-Xiang Chen[1,2] , Ji Shen[1,2] , Claudio Marchesi[3,4], Marco Scambelluri[5], Li-Ping Qin[1,2], Vicente López Sánchez-Vizcaíno[6] , José Alberto Padrón-Navarta[3,7] , Manuel D. Menzel[3] , and Carlos J. Garrido[3]

[1]CAS Key Laboratory of Crust-Mantle Materials and Environments, School of Earth and Space Sciences, University of Science and Technology of China, Hefei, China, [2]CAS Center for Excellence in Comparative Planetology, University of Science and Technology of China, Hefei, China, [3]Instituto Andaluz de Ciencias de la Tierra (IACT), CSIC-UGR, Granada, Spain, [4]Departamento de Mineralogía y Petrología, Facultad de Ciencias, Universidad de Granada, Granada, Spain, [5]Dipartimento di Scienze della Terra, Ambiente e Vita, Università di Genova, Genoa, Italy, [6]Departamento de Geología, Unidad Asociada al IACT, CSIC-UGR, Escuela Politécnica Superior, Universidad de Jaén, Linares (Jaén), Spain, [7]Géosciences Montpellier, UMR 5243, CNRS-Université Montpellier II, Montpellier, France

Abstract Fluids released through the dehydration of serpentinite can be rich in Cl⁻, which enables the significant mobility of Cr in subduction zones. However, the Cr isotope behavior accompanying the mobility of Cr during serpentinite dehydration is still poorly constrained. Here, we report high-precision Cr isotope data for a unique suite of serpentinites that represent metamorphic products at different depths in oceanic subduction zones. Low-grade serpentinites affected by significant Cr loss during serpentinization exhibit remarkably higher δ^{53}Cr, while samples with Cr contents $> \sim 1{,}800$ ppm typically preserve mantle-like δ^{53}Cr. Antigorite serpentinites have an average δ^{53}Cr value of $-0.17‰ \pm 0.19‰$ ($n = 12$, 2SD), which is statistically lower than those of low-grade serpentinite ($-0.05‰ \pm 0.30‰$, $n = 80$, 2SD) and higher-grade chlorite harzburgite ($-0.10‰ \pm 0.27‰$, $n = 22$, 2SD). This suggests that resolvable Cr isotope fractionation occurs during serpentinite dehydration, which is explained by the variability of Cr isotope behavior in the presence of Cl-bearing fluids at different dehydration stages. No obvious Cr isotope fractionation was found during chlorite harzburgite dehydration, probably related to the limited Cr mobility in a Cl-poor fluid. Other processes, such as melt extraction, external fluid influx and retrograde metamorphism, have negligible effects on the Cr isotope systematics of meta-serpentinites. Fluids released by serpentinite dehydration may have a great effect on the Cr isotope heterogeneity of mantle wedge peridotites and arc magmas.

Plain Language Summary Serpentinite plays an important role in crust–mantle interaction and arc magmatism in oceanic subduction zones. Serpentinite-derived fluids potentially mobilize Cr in the form of Cl complexes. However, there is limited information available about the Cr isotope compositions of subducted serpentinites, hindering the understanding of Cr isotope behavior during the dehydration of serpentinite. Here, we first report high-precision Cr isotope data for a unique suite of (meta-)serpentinite that encompasses low-pressure oceanic serpentinite to metamorphic products of complete dehydration at great depth. Our results fill the gap in the Cr isotope composition of meta-serpentinites metamorphosed under diverse P–T conditions in oceanic subduction zones. We found that there is variable and significant Cr isotope fractionation during prograde dehydration of serpentinites. Such serpentinite-derived fluids may contribute to the Cr isotope heterogeneity of mantle wedge peridotites and arc magmas.

1. Introduction

Chromium is a redox-sensitive element that mainly occurs as Cr^{6+} and Cr^{3+} in Earth's surface environments and as Cr^{3+} and Cr^{2+} in crustal and mantle rocks (Berry et al., 2006; O'Neill & Berry, 2021; Qin & Wang, 2017). The moderate compatibility of Cr during partial melting results in higher Cr concentrations in residual mantle peridotites than in basaltic and felsic rocks. While Cr almost exclusively occurs as Cr^{3+} in mantle minerals (Shen et al., 2018), Cr^{2+} can exist in high-temperature mafic melts under low fO₂ conditions (O'Neill & Berry, 2021 and references therein). Many studies have been devoted to exploring Cr isotope behavior during magmatic processes. For example, studies on komatiite and basalt have revealed limited equilibrium Cr isotope fractionation during partial melting and magmatic evolution (δ^{53}Cr variation
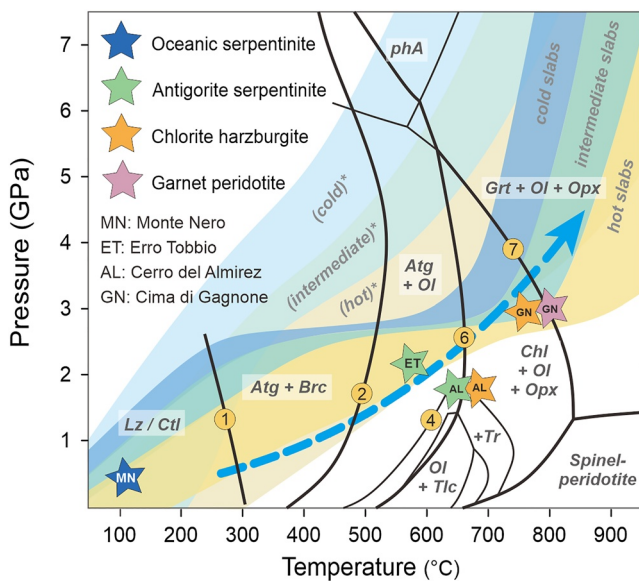
Figure 1. Computed *P–T* phase relations in subducted serpentinite (modified after Menzel et al., 2019, 2020) showing the peak *P–T* conditions of samples from the different localities in this work. The numbers on each curve refer to the mineral reactions listed in the text. Yellow, green and blue bands and lighter bands with * are the *P–T* trajectories of hot, intermediate and cold slabs at the slab-mantle interface and at the Moho depth within the slab after the thermal models of Syracuse et al. (2010), respectively. The blue dashed arrow shows the average metamorphic field gradient of subducted lithologies from exhumed metamorphic terranes (Penniston-Dorland et al., 2015).

<0.1‰, $\delta^{53}Cr = [(^{53}Cr/^{52}Cr)_{sample}/(^{53}Cr/^{52}Cr)_{SRM979} - 1] \times 1,000$; Bonnand et al., 2016, 2020; Jerram et al., 2020; Ma et al., 2022; Ping et al., 2022; Shen et al., 2018, 2020; Wagner et al., 2021). Investigations on mantle xenoliths found that melt percolation could lead to significant Cr isotope fractionation (Jerram et al., 2022; Xia et al., 2017). In contrast, Cr isotope behavior during metamorphism remains poorly constrained (Farkaš et al., 2013; Shen et al., 2015, 2021; Wang et al., 2016), as Cr^{3+} is commonly thought to be immobile due to its low solubility in aqueous fluids. However, several field observations of mafic rocks and Cr-rich veins manifest significant Cr mobility at crustal and mantle depths (e.g., Akizawa et al., 2016; Angiboust et al., 2014; Haws et al., 2021; Marshall et al., 2003; Spandler et al., 2011). In fact, it has been documented that Cr^{3+} can be mobilized in fluids with organic or inorganic ligands (Babechuk et al., 2017; Klein-Bendavid et al., 2011; McClain & Maher, 2016; Saad et al., 2017; Watenphul et al., 2014). Experimental studies have shown that fluids with high Cl contents can greatly facilitate Cr mobility (Klein-Bendavid et al., 2011; Watenphul et al., 2014). The model simulation of Huang et al. (2019) revealed that the Cr concentration in Cl-rich fluids is much higher than that in Cl-poor fluids. Importantly, Cr mobility in the presence of Cl ligands can be accompanied by remarkable Cr isotope fractionation (Babechuk et al., 2018; Larsen et al., 2016).

Serpentinites are widely considered key agents in geodynamic and geochemical processes in subduction zones (Deschamps et al., 2013; Scambelluri et al., 2004, 2019; Spandler & Pirard, 2013). Serpentinite dehydration in subduction zones not only modifies the geochemical composition of the subducting slab, but also transfers unique geochemical signatures to the overlying mantle wedge (e.g., Alt et al., 2012; Harvey et al., 2014; Scambelluri & Tonarini, 2012; Shen et al., 2021; Tonarini et al., 2011) and plays a key role in the oxidation of arc magmas (e.g., Debret et al., 2020; Padrón-Navarta et al., 2023; Y. X. Zhang et al., 2021). As serpentinite dehydration can generate Cl-rich fluids (Kendrick et al., 2011, 2018; Scambelluri et al., 1997, 2004, 2015), such a process is expected to not only release volatiles and fluid-mobile elements (FMEs) but also potentially mobilize Cr. Whether Cr mobilization during serpentinite dehydration would fractionate Cr isotopes is of particular interest. This is because serpentinite is a key Cr host in subduction zones, and thus its dehydration has a great bearing on the Cr isotope systematics in both hydrated mantle wedge peridotites and arc magmas, which is still unknown thus far. Given that subducted serpentinites often undergo multistage dehydration during their prograde evolution, a full understanding of Cr isotope behavior at different metamorphic stages requires a comprehensive investigation of samples exhumed from different depths of subduction zones.

In this study, we present high-precision Cr isotope data for a unique sample suite, filling the gap in the $\delta^{53}Cr$ values of serpentinites metamorphosed under diverse *P–T* conditions. The samples encompass low-pressure oceanic serpentinite to products of complete dehydration at great depths and thus provide new insights into Cr isotope behavior during various stages of serpentinite dehydration in oceanic subduction zones.

2. Geological Background and Samples

The samples investigated here include oceanic serpentinite from ophiolites, antigorite serpentinite, chlorite harzburgite, and garnet peridotite from exhumed palaeo-subduction metamorphic terrains (Figure 1). The ultramafic rocks in different massifs represent the remnants of previous lithospheric mantle that was affected by Alpine metamorphism. The eclogite-facies massifs record prograde evolution along the *P–T* path of subduction zones, providing ideal targets to investigate Cr isotope behavior during the prograde dehydration of serpentinites in subduction settings. The sample localities, mineral assemblages and chemical compositions have been previously reported in detail (Garrido et al., 2005; Halama et al., 2012; Marchesi et al., 2013; Padrón-Navarta et al., 2011; Scambelluri et al., 2001, 2014), and the chemical compositions for individual samples can be found in Table S1 in Supporting Information S1.

2.1. Monte Nero, Northern Apennine, Italy

The Northern Apennine ophiolites are lithospheric mantle remnants of the Ligurian Tethys Ocean (Montanini, 2006). Peridotite in Monte Nero (MN, Figure 1) is mainly serpentinized fertile spinel lherzolite. Three representative samples that formed during the onset of oceanic serpentinization were investigated here (Halama et al., 2012; John et al., 2011).

2.2. Erro-Tobbio, Western Alps, Italy

The Erro-Tobbio (ET) unit of the Voltri Massif (Western Alps) is mainly composed of serpentinized lherzolite-dominated meta-peridotite and was metamorphosed under high-pressure (HP) conditions (peak conditions at approximately 2.0–2.5 GPa, 550–600°C, Figure 1) during Alpine subduction (Hoogerduijn Strating et al., 1993; Scambelluri et al., 2001). Early low-grade serpentinite is structurally preserved (ETF 1, ETF 3) and overgrown by undeformed HP antigorite serpentinite (Atg-serpentinite). These undeformed domains are in turn surrounded by mylonitic Atg-serpentinite. Both undeformed and mylonitic serpentinites are cut by olivine-bearing veins crystallized during dehydration of antigorite and brucite (Scambelluri et al., 1997, 2001). Olivine-rich vein ET 42 and its corresponding wall rock ET 42A were collected in low-strain domains, while chlorite-rich vein ETF 10 and its wall rock ETF 9 and ETF 11 were from the mylonite zone (Früh-Green et al., 2004; Scambelluri et al., 2001).

2.3. Cerro del Almirez, Betic Cordillera, Spain

The Cerro del Almirez (CdA) massif is the largest ultramafic body of the Nevado-Filábride complex within the Betic Cordillera (southern Spain). The ultramafic bodies in the Nevado-Filábride complex occur on top of a heterogeneous sheared rock sequence mainly comprising metasediments. The whole sequence was metamorphosed under eclogite-facies with peak conditions at approximately 670°C and 1.6–1.9 GPa (Bretscher et al., 2018; López Sánchez-Vizcaíno et al., 2005; Padrón-Navarta et al., 2010, 2011; Trommsdorff et al., 1998).

The massif is composed of two lithological domains. The upper one is composed of foliated Atg-serpentinite overlying a lower domain of chlorite harzburgite (Chl-harzburgite) (Padrón-Navarta et al., 2011; Trommsdorff et al., 1998). Locally, transitional lithologies sharply separate the two rock sequences and vary from Chl-serpentinite close to the overlying Atg-serpentinite to antigorite-chlorite-orthopyroxene-olivine rocks (Atg-Chl-Opx-Ol rock) towards Chl-harzburgite (Padrón-Navarta et al., 2011). The crystal preferred orientations and textures of Chl-harzburgite are consistent with orthopyroxene and olivine formed after Atg-serpentinite and do not preserve any relics of primary high-temperature mantle deformation that are commonly observed in variably serpentinized abyssal peridotites (Dilissen et al., 2018, 2021; Padrón-Navarta et al., 2015).

Several metamorphic reactions affected Atg-serpentinite during prograde metamorphism. The transition from low-grade chrysotile/lizardite to antigorite took place through the reaction: chrysotile/lizardite = antigorite + brucite (1). Widespread olivine in serpentinite results from the partial dehydration reaction: antigorite + brucite = olivine + H_2O (2) (Jabaloy-Sánchez et al., 2022, Figure 1). In clinopyroxene (diopside)-bearing Atg serpentinite, relict mantle clinopyroxene (Cpx-1) recrystallized to metamorphic clinopyroxene (Cpx-2) through the reaction Cpx-1 + olivine + antigorite = Cpx-2 + chlorite + Ti-clinohumite + H_2O (3) (López Sánchez-Vizcaíno et al., 2005). Tremolite commonly occurs coexisting with olivine, and it frequently rims diopside by the reaction diopside + antigorite = tremolite + olivine + H_2O (4) (Figure 1). Orthopyroxene-bearing Atg-serpentinite occurs as a few small (<4 m in thickness) lenses within the Chl-harzburgite sequence. Such unusual paragenesis originated from antigorite and talc dehydration in a Si-enriched serpentinite: antigorite + talc = orthopyroxene + H_2O (5) (Padrón-Navarta et al., 2010).

Chl-harzburgite records the final breakdown of antigorite via the reaction antigorite = olivine + enstatite + chlorite + H_2O (6) (Trommsdorff et al., 1998). The HP orthopyroxene-rich veins (Alm-11 and Alm-13/3v) are considered to have formed during such a reaction (John et al., 2011; Kendrick et al., 2018). Although Chl-harzburgite can be subdivided into spinifex-like, granofelsic and occasionally recrystallized ones based on textures, they have similar mineral assemblages and bulk compositions and were formed under analogous *P–T* conditions (Dilissen et al., 2018; Padrón-Navarta et al., 2011).

2.4. Cima di Gagnone, Central Alps, Switzerland

The Cima di Gagnone (CdG) massif is located in the Adula-Cima lunga unit, Central Alps. The Gagnone ultramafic bodies are narrowly spaced and surrounded by crustal rocks (Evans & Trommsdorff, 1978; Scambelluri et al., 2014). The ultramafic Chl-harzburgite and garnet peridotite (Grt-peridotite) underwent similar peak P–T conditions of ca. 720–800°C, <3 GPa or 800–850°C, ca. 3 GPa (Figure 1, Nimis & Trommsdorff, 2001; Scambelluri et al., 2014). Grt-peridotite records the final dehydration of serpentine followed by chlorite breakdown: chlorite + orthopyroxene $\pm$ diopside = garnet + olivine + H_2O (7) (Kendrick et al., 2018; Scambelluri et al., 2015). Detailed field occurrence and petrography of the samples studied here have been reported in Scambelluri et al. (2014).

3. Methods

3.1. Whole-Rock Trace Element Analysis

Whole-rock trace element compositions of MNS-2, MNS-3, MNS-4, Al08-07, and Al08-38 were measured at the Sample Solution Lab, Wuhan, China, using an Agilent 7700e inductively coupled plasma mass spectrometer (ICP-MS). Approximately 50 mg of sample powder was dissolved in a mixture of HNO_3-HF in a Teflon beaker at 190°C for complete digestion. After evaporation on a hotplate for dryness, it was redissolved in HNO_3 and evaporated. Then, the sample was dissolved in HNO_3 solution, and 1 mL of indium solution (1 ppm) was added as an internal standard. The final solution was diluted with 2% HNO_3 to 100 mL for analysis. To monitor the data quality, two international silicate materials (AGV-2 and BHVO-2) were measured as unknowns, the results of which are consistent with the recommended values (Table S1 in Supporting Information S1). Based on the results of reference materials and duplicate samples, the analytical precision and accuracy were mostly better than $\pm 10\%$. The procedural blanks for each element are mostly <0.01 ppb.

3.2. Whole-Rock Cr Isotope Analysis

Whole-rock Cr isotope compositions were measured at the CAS Key Laboratory of Crust-Mantle Materials and Environments at the University of Science and Technology of China (USTC), Hefei. The procedures of sample dissolution and column chemistry have been reported by Shen et al. (2018) and Q. Zhang et al. (2019). In brief, approximately 5 mg of rock powder was dissolved in a mixture of twice-distilled HF-HCl-HNO_3 in capped beakers on a hot plate at 130°C overnight. After the complete dissolution of the sample, the solution was evaporated and then completely redissolved in 1 mL 6 N HCl. The Cr concentrations of the sample solutions were determined by ICP-MS to ensure that the mass of Cr in the aliquot was 1 μg. Then, the solutions were mixed with an appropriate amount of the ^{50}Cr to ^{54}Cr double spike. The molar ratio of ^{50}Cr to ^{54}Cr and weight proportion between the double spike and sample solution followed Shen et al. (2018). Cr separation was achieved by two-step cation chromatography using Bio-Rad AG 50 W-X8 resin (200–400 mesh). The total procedure blank was <3 ng, which was negligible compared to the separated Cr from the sample (1 μg).

Purified Cr samples were analyzed by a Thermo Scientific Neptune Plus multicollector–ICP–MS instrument at USTC. The detailed analytical procedure followed Shen et al. (2018) and Q. Zhang et al. (2019). All the sample solutions were diluted with 2% HNO_3 to 200 ppb and introduced with an Aridus II™ desolvating nebulizer. The carrier gas was high purity argon without the addition of N_2 to minimize potential polyatomic interferences. Analyses were performed in medium- to high-resolution modes (5,500 < M/ΔM < 11,000). The ion intensities of Cr isotopes and relevant isobaric interferences were measured in static mode on Faraday collectors, and all isobaric interferences were carefully corrected (Q. Zhang et al., 2019). Prior to each analytical session, the spiked NIST SRM 3112a standard was analyzed. After every 4–5 sample measurements, the spiked internal standard (SCP) was analyzed to monitor data quality. During the whole analytical period, NIST 3112a and SCP yielded δ^{53}Cr values of $-0.09 \pm 0.04‰$ ($n = 11$) and $-0.03 \pm 0.04‰$ ($n = 46$), respectively, which are consistent with the reported long-term mean values of $-0.07 \pm 0.06‰$ and $-0.02 \pm 0.04‰$, respectively (Shen et al., 2021). The peridotite reference material JP-1 shows a δ^{53}Cr of $-0.10 \pm 0.03‰$ ($n = 5$), consistent with previous results (Bonnand et al., 2016, 2020).

4. Results

The δ^{53}Cr values are listed in Table 1, and a summary of δ^{53}Cr for meta-serpentinites and related reservoirs is shown in Table 2. The newly analyzed trace element results for MNS-2, MNS-3, MNS-4, Al08-07, and Al08-38,

Table 1
Cr Isotope Composition of the Studied (Meta-) Serpentinites

Sample	Lithology	Mineral assemblage	$\delta^{53}Cr$ (‰)	2sd	n	Cr (ppm)
Stage 0 oceanic serpentinite, *Monte Nero*						
MNS-2	Low-grade serpentinite	Ctl, Lz, Ol, Opx, Cpx, Chl, Spl	−0.09	0.02	3	2,468
MNS-3			−0.17	0.04	3	2,307
MNS-4			0.61	0.03	2	816
ETF1			−0.09	0.03	3	1,529
ETF3			−0.13	0.03	3	1,895
Stage 0–1 Atg-serpentinite and vein, *Erro Tobbio*						
ET42A	Atg-serpentinite	Atg, Ol, Ti-Chu, Di	−0.39	0.01	2	2,336
ET42	Olivine rich vein	Ol, Ti-Chu, Mag, Di	−0.03	0.05	2	689
ETF10	Chlorite rich vein	Chl, Ol, Di, Mag	−0.19	0.05	3	1,591
ETF9	Atg-serpentinite	Atg, Ol, Di, Chl	−0.04	0.06	3	1,940
ETF11			−0.16	0.03	3	1,948
Stage 1 Antigorite-serpentinite, *Cerro del Almirez*						
Al98-4b	Atg-serpentinite	Atg, Ol, Mag, Tr, Chl, Ti-Chu	−0.24	0.04	2	2,475
Al98-5a			−0.17	–	1	1,789
Al06-44a			−0.23	0.03	3	2,970
Al06-46			−0.15	0.02	3	2,394
Al95-17	Cpx-bearing Atg-serpentinite	Atg, Ol, Di, Mag, Tr, Chl, Ti-Chu	−0.17	0.04	3	929
Al96-17			−0.11	0.02	3	2,187
Al98-33b			−0.08	0.04	2	1,640
Al06-09a			−0.08	0.02	3	2,705
Al06-20a	Opx-bearing Atg-serpentinite	Atg, Ol, Opx, Tlc, Mag, Tr	−0.27	0.01	2	3,632
Al06-37a			0.20	0.04	3	3,481
Stage 1–2 Transitional Lithologies, *Cerro del Almirez*						
Al07-06	Chl-serpentinite	Atg, Chl, Ol, Opx, Tlc, Mag, Tr	−0.15	0.01	2	2,553
Al06-43	Atg-Chl-Opx-Ol rock	Atg, Chl, Ol, Opx, Tlc, Mag, Tr	−0.15	0.04	3	2,612
Al08-14a			0.06	0.06	2	1,986
Stage 2 Chlorite-harzburgite, *Cerro del Almirez*						
Al06-18	Granofelsic Chl-harzburgite	Ol, Opx, Chl, Mag, Tlc, Tr, Ti-Chu	0.01	0.05	2	3,603
Al08-07			−0.03	0.02	3	2,005
Al08-16			−0.14	0.02	2	2,897
Al08-38			0.14	0.02	3	1,657
Al06-16	Spinifex-like Chl-harzburgite	Ol, Opx, Chl, Mag, Tlc, Tr, Ti-Chu	−0.14	0.06	3	2,952
Al06-17			0.02	0.01	2	2,823
Al06-19			−0.07	0.03	2	2,801
Al98-23			−0.16	0.01	2	2,036
Al95-41			−0.02	0.01	2	1,562
Al95-42			−0.16	0.02	2	1,409
Al95-55			−0.14	0.04	3	1,715
Al95-34			−0.29	0.03	3	1,523
Al95-29			−0.05	0.01	3	1,229
Alm-1			0.06	0.05	3	2,178
Alm-6			−0.12	0.06	3	2,291

Table 1
Continued

Sample	Lithology	Mineral assemblage	δ^{53}Cr (‰)	2sd	n	Cr (ppm)
Al96-1a	Recrystallized Chl-harzburgite	Ol, Opx, Chl, Mag, Tlc, Tr, Ti-Chu	−0.16	0.01	2	816
Al96-1c			−0.19	0.02	3	1,204
Al06-03a			−0.15	0.01	2	2,560
Al06-05b			−0.45	0.04	2	3,027
Al06-30b			0.15	0.06	2	2,637
Alm-11	High-pressure vein	Opx, Ol, Chl, Mag	−0.08	0.01	2	3,470
Alm-13/3v			−0.32	0.01	2	2,770
Stage 2 Chlorite-harzburgite, *Cima di Gagnone*						
Mg163 09-07	Chl-harzburgite	Ol, Chl, Opx, Tlc, Tr, Cum, Mag	−0.08	0.01	2	2,668
Mg163 09-05			−0.16	0.04	2	2,668
Stage 3 Garnet peridotite, *Cima di Gagnone*						
Mg160 09-10G	Garnet peridotite	Ol, Opx, Grt, Di, Mag, Amp, Tr, Tlc	−0.15	0.04	3	2,258
Mg160 09-02			−0.15	0.03	2	2,737
Mg160 09-05			−0.05	0.02	2	2,532
Reference materials						
SCP			−0.03	0.04	46	
NIST-3112a			−0.09	0.04	11	
JP-1			−0.10	0.03	5	

Note. Mineral abbreviations are after Whitney and Evans (2010). The major and trace elements of the samples are listed in Table S1 in Supporting Information S1.

and detailed major and trace elements for other samples are summarized in Table S1 in Supporting Information S1. We also compiled the reported low-grade serpentinite in Table S2 in Supporting Information S1. The compositional data in Table 1, Tables S1 and S2 in Supporting Information S1 are available in Xiong et al. (2023).

The δ^{53}Cr values of oceanic serpentinites range from −0.17‰ to 0.61‰, in agreement with the literature results (Figure 2a). The olivine-rich vein from ET yields a δ^{53}Cr value of −0.03 ± 0.05‰ ($n = 2$, 2SD), higher than its corresponding wall-rock Atg-serpentinite with a δ^{53}Cr of −0.39 ± 0.01‰ ($n = 2$, 2SD). The chlorite-rich vein in the mylonite zone yields a δ^{53}Cr value of −0.19 ± 0.05‰ ($n = 3$, 2SD), and its corresponding wall rocks show δ^{53}Cr values of −0.16‰ and −0.04‰. The Almirez Atg-serpentinites have variable δ^{53}Cr values from −0.27‰ to 0.20‰. Among the subgroups, Atg-serpentinite, Cpx-bearing serpentinite and Opx-bearing serpentinite yield δ^{53}Cr values of −0.24‰ to −0.15‰ ($n = 4$), −0.17‰ to −0.08‰ ($n = 4$), and −0.27‰ to 0.20‰ ($n = 2$), respectively (Table 1). In the Chl-harzburgite group, the δ^{53}Cr values of the granofelsic, spinifex-like and recrystallized

Table 2
Cr Isotope Results for Different Reservoirs and the Studied (Meta-) Serpentinite

Type	δ^{53}Cr (‰)	Q1 (‰)	Q3 (‰)	Median (‰)	Mean (‰)	2SD (‰)	N
Pristine peridotite xenolith	−0.22 to 0.00	−0.15	−0.10	−0.12	−0.12	0.10	20
Peridotite xenolith	−0.51 to 0.75	−0.17	−0.05	−0.11	−0.09	0.33	94
Low-grade serpentinite	−0.35 to 0.61	−0.13	0.00	−0.08	−0.05	0.30	80
Atg-serpentinite	−0.39 to −0.04	−0.24	−0.10	−0.17	−0.17	0.19	12
Chl-harzburgite	−0.45 to 0.15	−0.16	−0.02	−0.12	−0.10	0.27	22
Low-grade serpentinite (Cr of 1,800–4,000 ppm)	−0.35 to 0.08	−0.17	−0.04	−0.10	−0.11	0.17	41
Atg-serpentinite (Cr of 1,800–4,000 ppm)	−0.39 to −0.04	−0.24	−0.11	−0.16	−0.18	0.22	9
Chl-harzburgite (Cr of 1,800–4,000 ppm)	−0.45 to 0.15	−0.15	0.01	−0.10	−0.09	0.28	14

Note. Q1 and Q3 refer to the lower and upper quartiles, respectively. The δ^{53}Cr values of the peridotite xenoliths are from Ping et al. (2022).
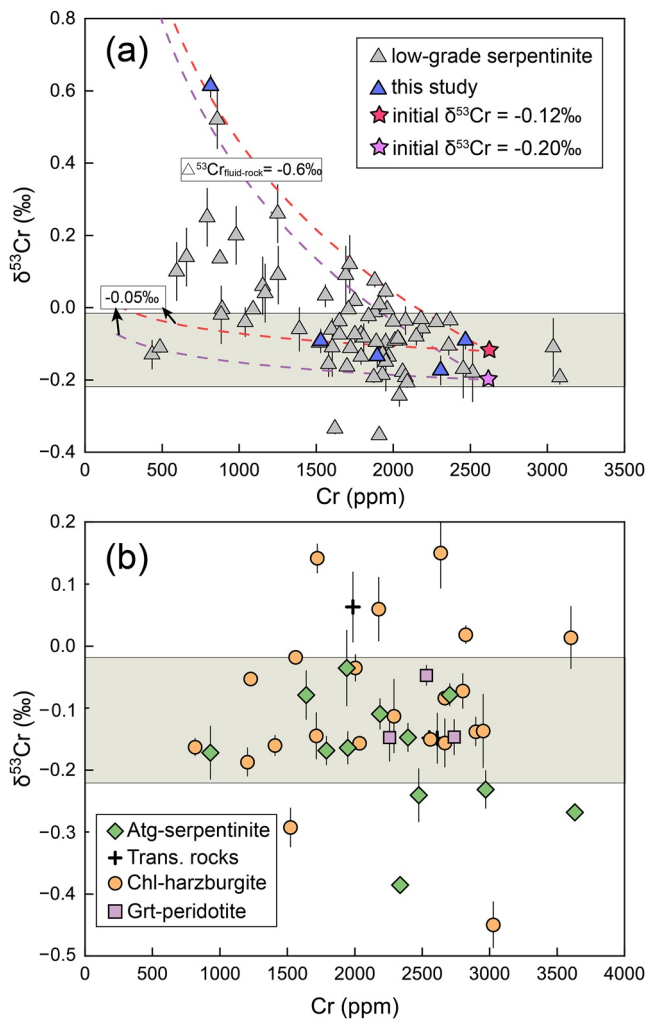
Figure 2. Plots of $\delta^{53}Cr$ versus Cr contents of (a) low-grade serpentinite and (b) higher-grade meta-serpentinite. The initial Cr content is from McDonough and Sun (1995). Two initial $\delta^{53}Cr$ values are used for Rayleigh fractionation modeling: $\delta^{53}Cr = -0.12‰$ (mean of bulk silicate Earth [BSE], Ping et al., 2022; Schoenberg et al., 2008) and $\delta^{53}Cr = -0.20‰$ used by Wang et al. (2016). Data sources: Kraemer et al. (2021), Novak et al. (2017, 2022), and Wang et al. (2016). Detailed data for the compiled low-grade serpentinite are shown in Table S2 in Supporting Information S1. The gray band denotes $\delta^{53}Cr$ values for the BSE, the same in other figures.

samples are $-0.14‰$ to $0.14‰$ ($n = 4$), $-0.29‰$ to $0.06‰$ ($n = 11$), and $-0.45‰$ to $0.15‰$ ($n = 5$), respectively. The syn-metamorphic Opx-rich veins Alm-11 and Alm-13/3v display $\delta^{53}Cr$ values of $-0.08 \pm 0.01‰$ ($n = 2$, 2SD) and $-0.32 \pm 0.01‰$ ($n = 2$, 2SD), respectively. The $\delta^{53}Cr$ values of Gagnone Chl-harzburgite range from $-0.16‰$ to $-0.08‰$ ($n = 2$), while those of Grt-peridotite range from $-0.15‰$ to $-0.05‰$ ($n = 3$).

To compare the data from the meta-serpentinites, we performed a statistical analysis of the samples. According to Shapiro normality tests, some rock types are not normally distributed, and therefore we used the non-parametric Mann–Whitney test to assess the potential differences among the $\delta^{53}Cr$ of various rock types. An Opx-bearing Atg-serpentinite with remarkably higher SiO_2 than others is considered an outlier and is excluded from further discussion (Figure S1 in Supporting Information S1). Because low-grade serpentinite with lower Cr contents can display fractionated $\delta^{53}Cr$ values (Figure 2a), samples with higher Cr contents of 1,800–4,000 ppm are also selected for comparison. The results are listed in Table S3 in Supporting Information S1.

At the 95% confidence level, the average $\delta^{53}Cr$ of low-grade serpentinites ($-0.05 \pm 0.30‰$, $n = 80$, 2SD) is statistically higher than that of bulk silicate Earth (BSE; $\delta^{53}Cr = -0.12 \pm 0.10‰$) ($p = 0.009$, Table S3 in Supporting Information S1). The average $\delta^{53}Cr$ of Atg-serpentinite ($-0.17 \pm 0.19‰$, $n = 12$, 2SD) is statistically lower than that of low-grade serpentinite ($p = 0.002$) and Chl-harzburgite ($-0.10 \pm 0.27‰$, $n = 22$, 2SD). Focusing on meta-serpentinite samples with Cr concentrations of 1,800–4,000 ppm, low-grade serpentinites have an average $\delta^{53}Cr$ of $-0.11 \pm 0.17‰$ ($n = 41$, 2SD), showing no significant difference compared to the BSE ($p = 0.358$) and peridotite xenolith ($p = 0.971$). Atg-serpentinite with an average $\delta^{53}Cr$ of $-0.18 \pm 0.22‰$ ($n = 9$, 2SD) is still statistically lower than low-grade serpentinite ($p = 0.044$) and Chl-harzburgite ($p = 0.047$) (Table S3 in Supporting Information S1).

5. Discussion

The presented sample suite spans a large $\delta^{53}Cr$ range of $\sim 1‰$. In addition, there are two outstanding observations among the (meta-)serpentinites: (a) low-grade serpentinites with Cr $< \sim 1,800$ ppm have significantly higher $\delta^{53}Cr$ values than those samples with Cr $> 1,800$ ppm (Figure 2a), whereas there is no clear trend between Cr concentrations and $\delta^{53}Cr$ values of mantle xenoliths (Jerram et al., 2022; Ping et al., 2022); (b) The studied Atg-serpentinites have lower average $\delta^{53}Cr$ value by $\sim 0.08‰$ than both low-grade serpentinites and Chl-harzburgites, regardless of whether the Cr contents are restricted to 1,800–4,000 ppm or not (Table 2; Figures 2b and 3). Notably, some meta-serpentinites yield low $\delta^{53}Cr$ that are rarely found in low-grade

serpentinite (Figure 2), and the obviously variable $\delta^{53}Cr$ values of fluid-induced veins from -0.32 to $-0.03‰$ imply that prograde serpentinite devolatilization could produce resolvable Cr isotope fractionation. Although these observations suggest the significant role of serpentinization and devolatilization in the Cr isotope systematics of the (meta-)serpentinites, other processes must be assessed first. These processes are (a) melt extraction/ percolation of mantle protoliths prior to serpentinization; (b) external fluid influx in the subduction zone; and (c) retrogression and rehydration during exhumation.

5.1. Effect of Mantle Melting and Melt-Peridotite Reaction

The chemical composition of peridotites prior to serpentinization is mainly the combined result of melt extraction and late refertilization (e.g., Bodinier & Godard, 2014; Niu, 2004). In the Al_2O_3/SiO_2 versus MgO/SiO_2 plot, the serpentinites follow a magmatic depletion trend and fall within the range of abyssal peridotites (Figure S2 in
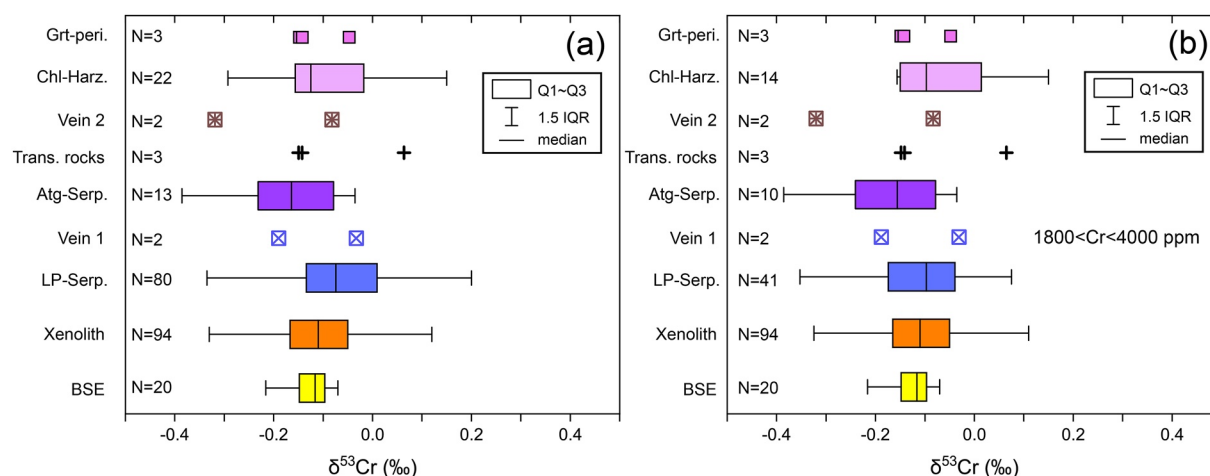
Figure 3. Boxplot of $\delta^{53}Cr$ for relevant reservoirs and samples in this study (a). Also shown is the boxplot of (meta-)serpentinites with Cr contents between 1,800 and 4,000 ppm (b). Data for bulk silicate Earth and peridotite xenoliths are from Jerram et al. (2022) and Ping et al. (2022).

Supporting Information S1). The good correlations between Al_2O_3, Sc, and V indicate that these elements mostly preserve the magmatic signature of the protolith (Figures 4a and 4b, see also Marchesi et al., 2013). There are no systematic differences among these elements for each group of meta-serpentinite. Similar to both peridotite xenoliths and abyssal peridotites worldwide, the Cr contents of the samples show no correlations with Al_2O_3 (Figure 4c). The vast Cr content heterogeneity is likely caused by different elemental behaviors during melt extraction under variable P–T–fO_2 conditions and local effects of melt–rock reactions (Bodinier & Godard, 2014; Liang & Elthon, 1990; Roeder & Reynolds, 1991).

Previous studies have shown that although melts have slightly lower $\delta^{53}Cr$ than peridotite ($\Delta^{53}Cr_{residue-melt} < 0.1‰$, Bonnand et al., 2020; Jerram et al., 2020; Ma et al., 2022; Shen et al., 2020), melt extraction has a rather limited effect on the Cr isotope composition of residual peridotites (<0.01‰, Jerram et al., 2022), as shown by the lack of correlations between Al_2O_3/SiO_2 and $\delta^{53}Cr$ (Figure 4d). In contrast, $\delta^{53}Cr$ variations in mantle rocks can be produced by later melt refertilization (Jerram et al., 2022; Xia et al., 2017). Under the Cr concentration gradient between ultramafic peridotites and percolated melts, kinetic exchange would lead to the preferential loss of isotopically lighter Cr into the melts, leaving residues with higher $\delta^{53}Cr$ values (Jerram et al., 2022; Xia et al., 2017). On the other hand, the direct contribution of low-$\delta^{53}Cr$ melts into the percolated peridotites may result in mantle rocks with lower $\delta^{53}Cr$ (Ping et al., 2022). A melt percolation process should display a correlation between $\delta^{53}Cr$ and incompatible elements (Jerram et al., 2022). Considering that the original REEs (except for La and Eu in some cases) of protoliths are commonly preserved during (de)serpentinization (Deschamps et al., 2013; Niu, 2004), REE ratios can be used as tracers for melt percolation (Pettke & Bretscher, 2022). The presented (meta-)serpentinites are generally depleted, and their $\delta^{53}Cr$ values show no correlations with $(Ce/Yb)_N$. Therefore, melt percolation cannot explain the systematic trend of the sample suite (Figure 4e).

5.2. Effect of External Fluid Influx in the Subduction Zone

During subduction, serpentinites could have experienced cryptic metasomatism by external fluids from crustal rocks, leading to the enrichment of FMEs and related isotopes (Cannaò et al., 2015; Debret et al., 2021; Garrido et al., 2005; López Sánchez-Vizcaíno et al., 2005). However, no systematic enrichment of FMEs among each group of samples is observed, and there are no correlations between $\delta^{53}Cr$ and FMEs of the meta-serpentinites (Figure 5). In fact, Cr abundances in oceanic crust (~320 ppm, White & Klein, 2014) and global subducting sediments (~70 ppm, Plank, 2014) are much lower than those of mantle peridotites and serpentinites (normally ~2,000–4,000 ppm, Figure 4c). Hence, from a mass balance perspective, the effect of interaction with crustal fluids on Cr isotope variations in subducted serpentinites is negligible.

5.3. Effect of Retrogression and Rehydration During Exhumation

Previous studies have emphasized the geochemical effect of retrogression during the exhumation of meta-serpentinites (e.g., Pettke & Bretscher, 2022). Among the sample suites, retrogression has been observed in transitional lithologies
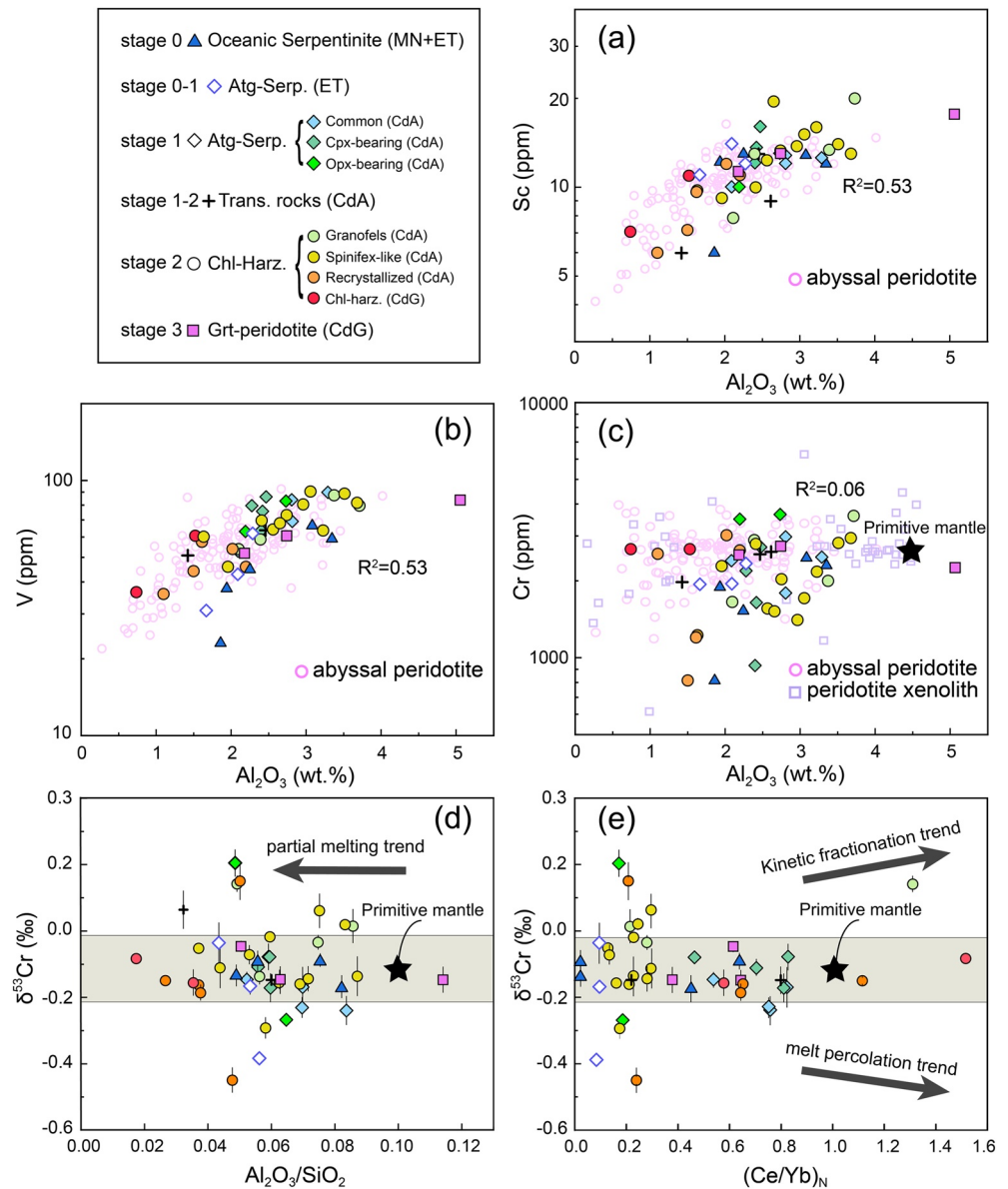
Figure 4. Plots of element and Cr isotope variations for the studied samples. Panels (a–c) also show the coefficient of determination (R^2) of the linear fitting for the studied samples. Values for primitive mantle in (c–e) are from McDonough and Sun (1995). Data sources: abyssal peridotites, Niu (2004); mantle peridotite xenoliths, Jerram et al. (2022) and Ping et al. (2022).

and Chl-harzburgites from CdA (Bretscher et al., 2018; Debret et al., 2015; Padrón-Navarta et al., 2011) and a Grt-peridotite from CdG (Scambelluri et al., 2014). The main hydrous mineral in Atg-serpentinite is antigorite, while that in Chl-harzburgite is chlorite. Meanwhile, antigorite and chlorite are the main Al-bearing minerals in both rock types, dominating their bulk Al_2O_3 contents. As such, the theoretical H_2O stored by peak assemblages can be assessed by the bulk rock Al_2O_3 contents (Bretscher et al., 2018; Pettke & Bretscher, 2022). For Atg-serpentinite, the general match of measured loss on ignition (LOI) and predicted range suggests the minor effect of retrogression (Figure 6a), in agreement with previous observations (Bretscher et al., 2018; Padrón-Navarta et al., 2011). In contrast, the LOI of Chl-harzburgites is significantly higher than the predicted range (Figure 6b), manifesting the presence of later-formed serpentine and talc (Bretscher et al., 2018; Pettke & Bretscher, 2022; Vieira Duarte et al., 2021).

If retrogression upon exhumation played a role in the Cr isotope composition of the meta-serpentinites, a systematic difference in $\delta^{53}Cr$ between each group with various extents of rehydration would be expected, which is,

Figure 5. Plots of $\delta^{53}Cr$ versus (a) Rb/Th, (b) U/Th, (c) Sr/Y and (d) Ba/Nb of the subducted serpentinites.

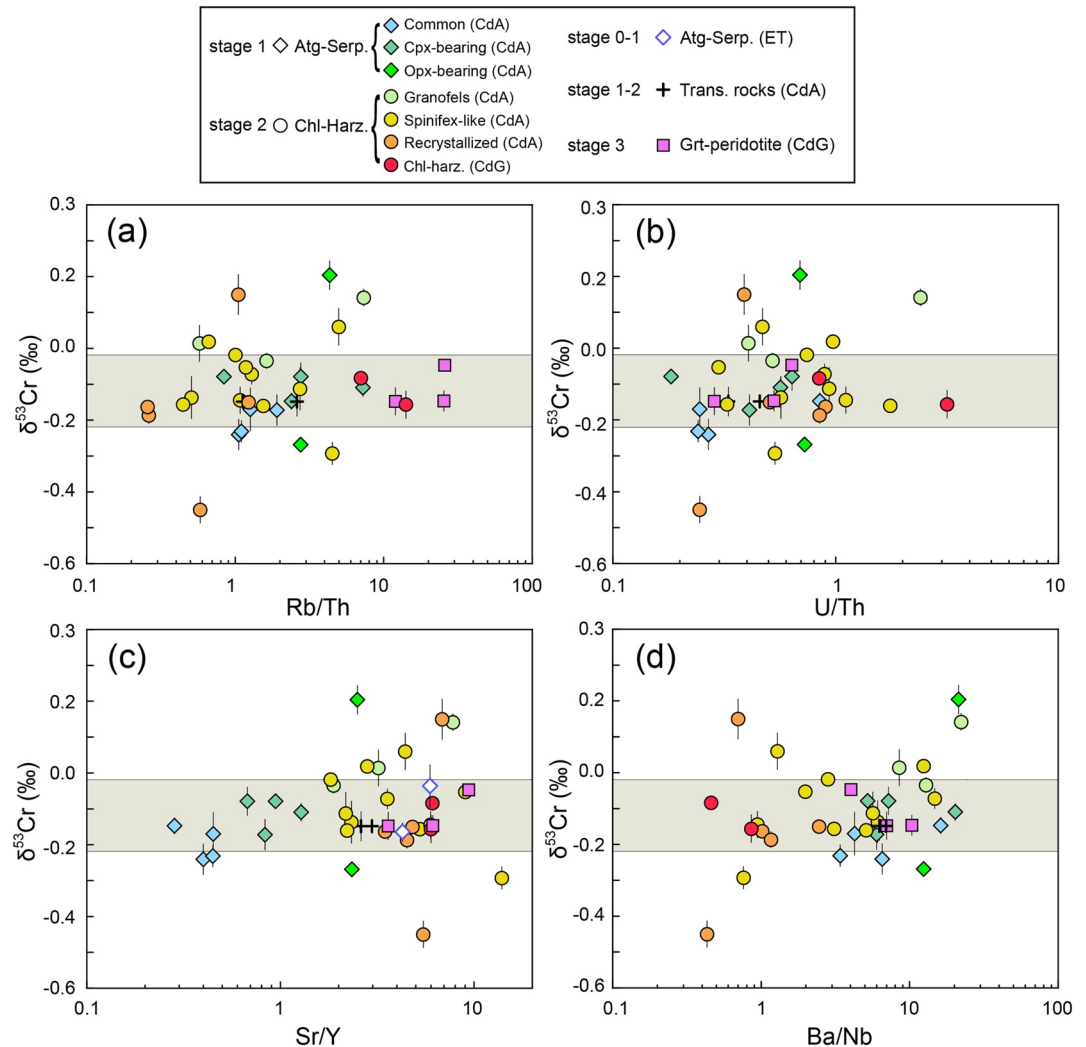however, not observed (Figure 6). Therefore, late retrograde reactions have an insignificant effect on the Cr isotope systematics, in agreement with previous observations (Shen et al., 2015).

In summary, magmatic processes, external fluid metasomatism and retrogression cannot explain the systematic trends of (meta-)serpentinites. Alternatively, the observed variation in $\delta^{53}Cr$ of (meta-)serpentinite is most likely associated with Cr isotope fractionation during serpentinization and prograde devolatilization.

5.4. Cr Isotope Behavior During Seafloor Serpentinization and Prograde Serpentinite Dehydration

5.4.1. Oceanic Serpentinization Stage (Stage 0)

The studied oceanic serpentinites display a large $\delta^{53}Cr$ variation from BSE-like to a much higher value of 0.61‰, consistent with previous results. In addition, the compiled low-grade serpentinites show elevated $\delta^{53}Cr$ at low Cr concentrations (Figure 2a). Because the extent of serpentinization and late weathering have negligible effects on the Cr isotope composition of serpentinite (Novak et al., 2022), such a trend was previously explained either by redox-related serpentinization or by the loss of isotopically lighter Cr^{3+} during serpentinization (non-redox-related) (Farkaš et al., 2013; Kraemer et al., 2021; Wang et al., 2016). The redox-related interpretation involves the oxidation of immobile Cr^{3+} into soluble Cr^{6+} that is lost during serpentinization. Although the oxidation of Cr^{3+} to Cr^{6+} during serpentinization can be feasible in some cases (Oze et al., 2016), the accompanying Cr isotope behavior, which is crucial for the isotope composition of the residues, is still poorly constrained. Previous experimental
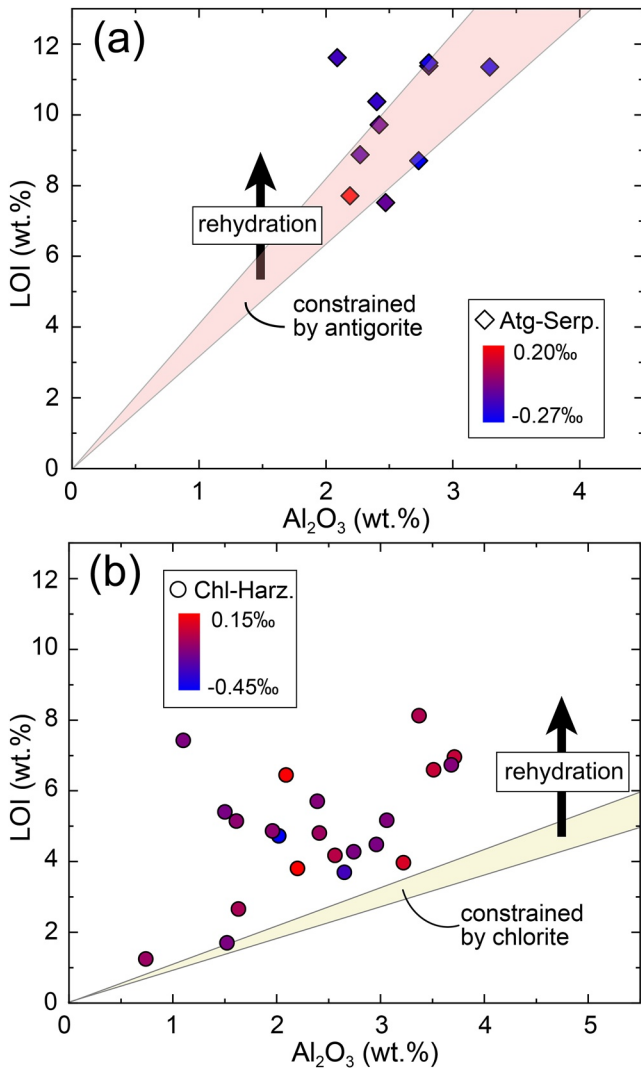
Figure 6. Plot of loss on ignition (LOI) versus Al_2O_3 for Atg-serpentinite (a) and Chl-harzburgite (b). The pink area in (a) and yellow area in (b) are constrained by the compositions of antigorite and chlorite, respectively (see text for detail). Rehydration of olivine and/or pyroxene to serpentine and talc would increase the bulk LOI. Compositional data for antigorite and chlorite are from Padrón-Navarta et al. (2011).

studies documented highly variable Cr isotope fractionation factors (even opposite fractionation directions) during the oxidation of Cr^{3+} to Cr^{6+} (Bain & Bullen, 2005; Zink et al., 2010), which are significantly different from the calculated equilibrium fractionation factors (Schauble et al., 2004). Hence, the behavior of Cr isotopes in the redox process may be very complex and needs further constraints (Wang et al., 2015). Alternatively, more recent studies found that significant Cr isotope fractionation can be induced by the removal of Cr^{3+} in the presence of complexing ligands (Babechuk et al., 2017, 2018; McClain & Maher, 2016; Saad et al., 2017). In this regard, the observed trend in Figure 2a can be due to the removal of isotopically light Cr during serpentinization (Babechuk et al., 2017, 2018; Wang et al., 2016). The Rayleigh fractionation modeling shows that a fractionation factor between fluid and serpentinite ($\Delta^{53}Cr_{fluid-rock}$) of −0.05 to −0.6‰ is needed to account for the range of low-grade serpentinites (Figure 2a).

Nevertheless, higher $\delta^{53}Cr$ values in low-grade oceanic serpentinites are only observed in samples with lower Cr contents (Figure 2a). When focusing on samples with higher Cr contents of 1,800–4,000 ppm, their $\delta^{53}Cr$ values are consistent with those of peridotite xenoliths (Figure 3b). This suggests that resolvable Cr isotope fractionation during serpentinization requires significant loss of Cr.

5.4.2. From Low-Grade Serpentinite to Atg-Serpentinite (Stage 0–1)

The shallow and low-temperature origin of the ET and Almirez serpentinites has been confirmed by previous field and geochemical studies (Garrido et al., 2005; Kendrick et al., 2011; Marchesi et al., 2013; Scambelluri et al., 2001). The higher grade Atg-serpentinite formed through a phase transition from chrysotile/lizardite to antigorite. The absence of brucite and the presence of olivine may further indicate the occurrence of the brucite-out reaction at higher $P–T$ conditions. These processes lead to the release of approximately 3 wt.% fluids (Figure 7). Atg-serpentinite has an average $\delta^{53}Cr$ of −0.17 ± 0.19‰ ($n = 12$, 2SD), which is statistically lower than that of low-grade serpentinite of −0.05 ± 0.30‰ ($n = 80$, 2SD) (Figure 3). For samples with Cr contents of 1,800–4,000 ppm, such a difference is still significant (Table S3 in Supporting Information S1). The resolvable lighter Cr isotope compositions of Atg-serpentinite cannot be explained by Cr loss during serpentinization, which would otherwise result in enrichment of heavier Cr in the residues (Figure 2a). In fact, for both Atg-serpentinite and Chl-harzburgite, the mean $\delta^{53}Cr$ of samples with restricted Cr contents (1,800–4,000 ppm) is comparable to that of samples with unrestricted Cr contents (Table 2), indicating that Cr loss during initial serpentinization had an insignificant effect on the Cr isotope compositions of the present higher grade rock types (Figure 2b). Instead, the lower $\delta^{53}Cr$ values of Atg-serpentinite than those of the low-grade serpentinites suggest isotopic fractionation during prograde metamorphism.

In Atg-serpentinite, almost all Cr is hosted by antigorite and magnetite (Padrón-Navarta et al., 2011; Vieira Duarte et al., 2021). Cr is partitioned together with other trivalent cations, such as Al^{3+} in antigorite (Padrón-Navarta et al., 2013), while it substitutes octahedral Fe^{3+} in magnetite. The transformation of lizardite into antigorite, despite associated water loss, presumably would not remarkably fractionate Cr isotopes as they belong to the same serpentine group. Because antigorite contains much less Fe^{3+} than lizardite (Evans et al., 2012), prograde serpentine phase transformation would facilitate magnetite crystallization for excess Fe^{3+} (Vieira Duarte et al., 2021). As a result of more Fe^{3+} competing octahedral positions in magnetite, the corresponding Cr contents would be much lower. Indeed, Vieira Duarte et al. (2021) found that the Cr contents of the magnetite formed at this stage ($Cr_2O_3 < 6$ wt.%) are much lower than those of relict magnetite (Cr_2O_3 up to 10 wt.%). The ionic model calculation predicted that spinel is isotopically heavier in Cr than other mantle minerals (Cpx, Opx and
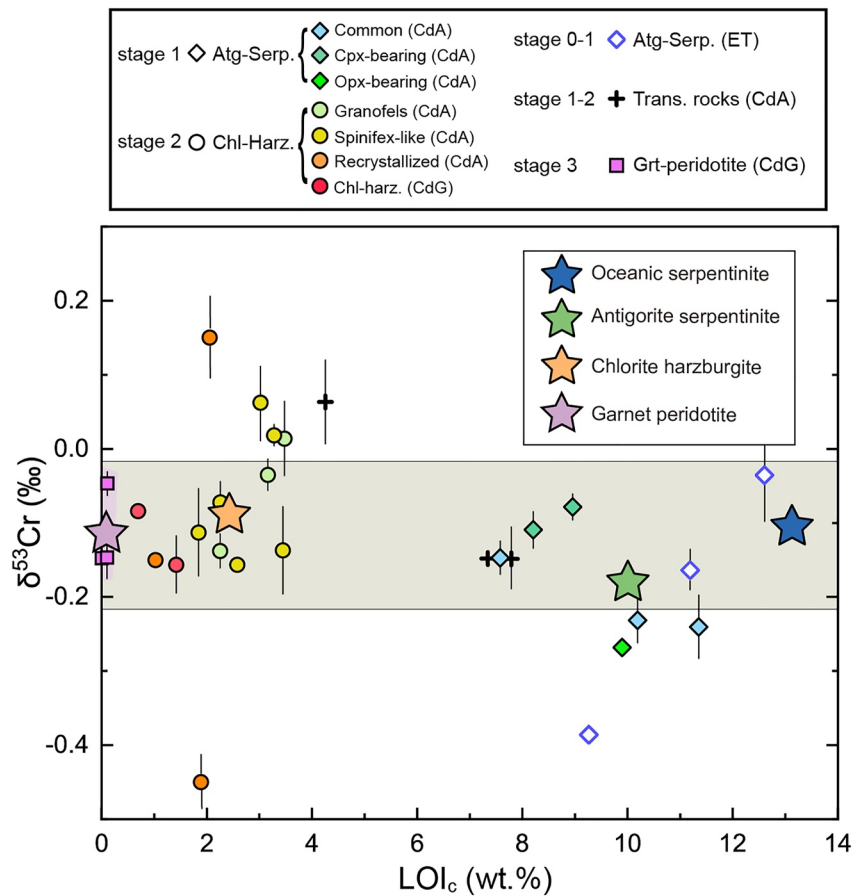
Figure 7. $\delta^{53}Cr$ versus LOI_c for the studied samples with Cr contents of 1,800–4,000 ppm. To remove the effect of rehydration, the shown loss on ignition (LOI) values are calculated based on peak assemblages (LOI_c); see text for details. Stars represent the average values of each rock type. The initial low-grade serpentinite is assumed to contain 13 wt.% H_2O.

Ol) (Shen et al., 2018). Magnetite with spinel-like crystallography should also be enriched in heavier Cr. Novak et al. (2017) showed that the Cr-magnetite-rich part in serpentinite displays a much higher $\delta^{53}Cr$ of +0.4‰ than the residual fraction of −0.29‰. Importantly, serpentinite phase transformation is accompanied by the release of high-salinity fluids (<50 wt.% $NaCl_{equiv.}$, Scambelluri et al., 1997, 2004; Kendrick et al., 2011), which effectively enhances Cr mobility by up to several orders of magnitude (Huang et al., 2019; Klein-BenDavid et al., 2011; Watenphul et al., 2014).

Therefore, we infer that during the formation of Atg-serpentinite, Cr was redistributed in both antigorite and magnetite recrystallization. The acquisition of much more Fe^{3+} in magnetite facilitates an intense redistribution and partial loss of heavier Cr, as Cr is more readily mobile in the presence of high-salinity fluids (Crossley et al., 2017; Huang et al., 2019; Watenphul et al., 2014). This hypothesis is strengthened by the remarkably higher $\delta^{53}Cr$ of a fluid-induced vein (ET42) than its serpentinite wall rock (ET42A) from ET. The other vein (ETF10) in the mylonite zone contains abundant chlorite that is not found in the undeformed veins (Scambelluri et al., 2001). Considering that both its trace element composition and $\delta^{18}O$ value are different from those of other HP veins (Früh-Green et al., 2004; Scambelluri et al., 2001), it seems that such a vein sample in the high-strain domain records a much more complex process.

For a better constraint, we performed batch and Rayleigh distillation models to estimate Cr isotope variation during serpentinite dehydration at this stage, following the methods of Pons et al. (2016) (Figure 8a). As there is no available Cr isotope fractionation factor between fluid and rock for the meta-serpentinite system, we used paired vein-wall rock samples to estimate the fractionation factor (Figure 7a). The initial rock value is the mean $\delta^{53}Cr$ of low-grade serpentinite with Cr contents of 1,800–4,000 ppm. The results show that with a fluid–rock fractionation factor of ~0.3‰, a loss of ~15% Cr from the original serpentinite is needed for the mean $\delta^{53}Cr$
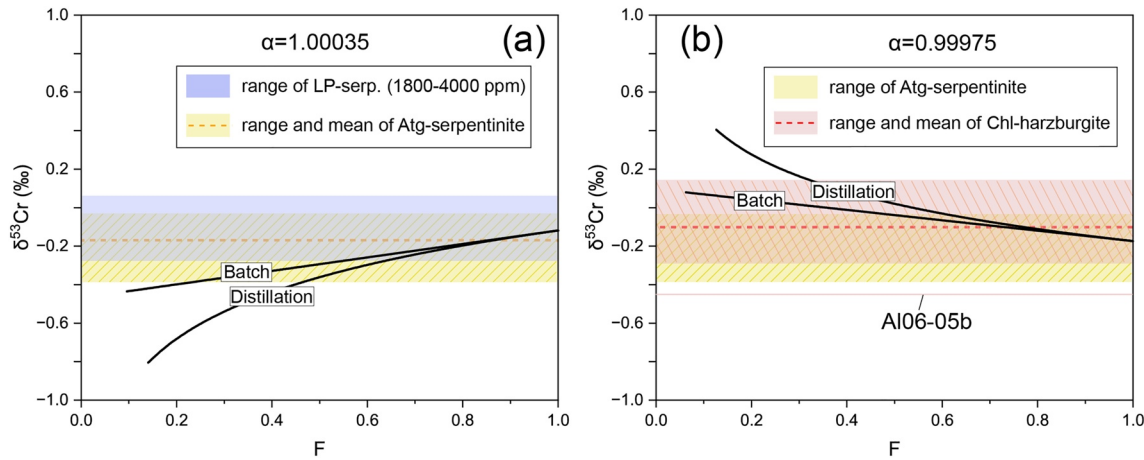
Figure 8. Batch and Rayleigh distillation models for the evolution of $\delta^{53}Cr$ during serpentinite dehydration from stage 0–1 (a) to stage 1–2 (b). In the batch model, the $\delta^{53}Cr$ of the final rock is calculated by $\delta^{53}Cr_{initial} = \delta^{53}Cr_{final} \times F + \delta^{53}Cr_{fluid} \times (1 - F)$ and $\delta^{53}Cr_{fluid} - \delta^{53}Cr_{final} = 1{,}000 \times \ln\alpha$, while the $\delta^{53}Cr$ value of the final rock in the Rayleigh model is calculated by $\delta^{53}Cr_{final} - \delta^{53}Cr_{initial} = (1{,}000 + \delta^{53}Cr_{initial}) \times (F^{(\alpha-1)} - 1)$, where F is the fraction of Cr in the residue. The fractionation factor α between fluid and meta-serpentinite for each stage is estimated based on the $\delta^{53}Cr$ of the vein and its wall rock. The initial rock values are the mean $\delta^{53}Cr$ of low-grade serpentinite with Cr contents of 1,800–4,000 ppm in panel (a) and the mean $\delta^{53}Cr$ of Atg-serpentinite in panel (b).

of Atg-serpentinite. The average anhydrous Cr concentration of low-grade serpentinite is ~2,600 ppm (assuming ~13 wt.% water), while that of the Atg-serpentinites is ~2,400 ppm. In addition to their loss of ~2–6 wt.% water (m_f), the remaining Cr fraction at this stage can be estimated by $C_{final}/C_{initial} \times (1 - m_f) \approx 0.87 - 0.90$ (Pons et al., 2016). Considering the local variability of both Cr content and $\delta^{53}Cr$, the preferential loss of heavier Cr reasonably accounts for the lower average $\delta^{53}Cr$ of Atg-serpentinite than that of low-grade serpentinite.

5.4.3. From Atg-Serpentinite to Chl-Harzburgite (Stage 1–2)

The contact boundary between Atg-serpentinite and Chl-harzburgite in Almirez shows no signs of tectonic discontinuity (Padrón-Navarta et al., 2011). Transitional lithologies at the contact steadily show the disappearance of antigorite and the growth of orthopyroxene and olivine. The contact is commonly interpreted as representing a reaction front formed by subduction HP dehydration of Atg-serpentinite to produce Chl-harzburgite (Garrido et al., 2005; Marchesi et al., 2013; Padrón-Navarta et al., 2011; Trommsdorff et al., 1998). It is also proposed that this Atg-out front corresponds to an oxidation serpentinization front, separating the serpentinite protoliths of Atg-serpentinite and Chl-harzburgite with variable compositions that were caused by different types of melt refertilization and extents of seafloor serpentinization (Bretscher et al., 2018; Pettke & Bretscher, 2022; Piccolli et al., 2019). As mentioned above, both rock types show overlapping Al_2O_3, V, and Sc, indicating a similar magmatic history (Figure 4), which is also supported by the lack of systematic differences in Fe isotopes among both rock types (Debret et al., 2021). In addition to textural variations pointing to metamorphic growth of Chl-harzburgite after a serpentinite protolith (Dilissen et al., 2018, 2021; Padrón-Navarta et al., 2015), thermodynamic modeling shows that open-system serpentinite dehydration can account for the oxidation differences between the two types of rocks (Padrón-Navarta et al., 2023). Therefore, the observed higher average $\delta^{53}Cr$ of the Chl-harzburgites than that of Atg-serpentinites by ~0.08‰ cannot be dominated by the heterogeneity of the protolith. Instead, in view of the large amounts of released aqueous fluids (~8 wt.%, Figure 8), a more feasible scenario would be that Cr was also mobile during metamorphic dehydration of Atg-serpentinite to form Chl-harzburgite, inducing Cr isotope fractionation at this stage. Resolvable fluid–rock Cr isotope fractionation is evidenced by the obviously low $\delta^{53}Cr$ in an HP syn-metamorphic vein (Alm-13/3v).

In Almirez, the antigorite breakdown reaction leads to the formation of Cr-rich magnetite, and mass balance calculations reveal that magnetite in Chl-harzburgite contains more bulk Cr than that in Atg-serpentinite (Vieira Duarte et al., 2021). This means that the Cr excess from the breakdown of antigorite would be accommodated in magnetite (Vieira Duarte et al., 2021). Consequently, the stabilization of magnetite prevents the loss of isotopically heavy Cr during intense Cr redistribution. We model the possible $\delta^{53}Cr$ variation at this stage, assuming that the initial material value is the average $\delta^{53}Cr$ of Atg-serpentinite (Figure 8b). The fractionation factor is inferred from isotope compositions of the vein Alm-13/3v and adjacent Chl-harzburgite samples (Alm-1, Alm-6)

(Halama et al., 2012). The results show that with a fluid–rock fractionation factor of −0.25‰, a loss of ∼20% Cr from the initial rock can match the observed average $\delta^{53}Cr$ of Chl-harzburgite. As the average Cr content of Chl-harzburgite is ∼2,200 ppm, and in addition to their loss of ∼8 wt.% water at this stage (Figure 7), the remaining Cr fraction is approximately $C_{final}/C_{initial} \times 0.92 \approx 0.84$. In view of the variability in both Cr content and $\delta^{53}Cr$, it is reasonable to infer that the lower $\delta^{53}Cr$ of Atg-serpentinite than that of Chl-harzburgite is caused by the preferential loss of isotopically lighter Cr during Cr redistribution in the presence of Cl-bearing fluids. Such a process cannot explain Chl-harzburgite Al06-05b with a very low $\delta^{53}Cr$ value of $<−0.4‰$ (Figure 8b). Given that this sample shows no evidence of melt percolation (Figure 4e), its low $\delta^{53}Cr$ may be related to interaction with fluids with isotopically lighter Cr at this stage or to other unknown processes.

5.4.4. From Chl-Harzburgite to Grt-Peridotite (Stage 2–3)

Grt-peridotites from CdG have Cr isotope compositions similar to those of Chl-harzburgite. During stage 2–3, the transition from Chl-harzburgite to Grt-peridotite releases a limited amount of fluid from the breakdown of chlorite compared to that from antigorite breakdown (Figure 7). The study on Gagnone meta-peridotite documented a much lower Cl concentration in fluids released from chlorite breakdown (Scambelluri et al., 2015). This is further reinforced by the similar bulk Cl concentrations in Chl-harzburgite (36 ppm) and Grt-peridotite (∼40 ppm) from Gagnone (Kendrick et al., 2018). The lack of resolvable Cr isotope fractionation from Chl-harzburgite to Grt-peridotite is likely ascribed to the limited Cr mobility due to the lack of aqueous Cl complexes in fluids.

6. Implications

The scarcity of Cr isotope data in subduction-related metamorphic rocks has hindered our understanding of Cr isotope behavior during metamorphic devolatilization reactions in subduction zones (Shen et al., 2015, 2021; Wang et al., 2016). Based on a unique sample suite, this study aims to fill the gap in the $\delta^{53}Cr$ values of serpentinites metamorphosed under diverse P–T conditions in subduction zones. The fact that higher $\delta^{53}Cr$ of low-grade serpentinite always correlates with lower Cr contents while samples with higher Cr contents (>∼1,800 ppm) typically have BSE-like compositions indicates that the positive shift in $\delta^{53}Cr$ cannot be the result of isotope exchange with isotopically heavier seawater (Wang et al., 2016). The most straightforward interpretation is that isotopically lighter Cr is preferentially removed during serpentinization. This scenario implies that the fluids involved in serpentinization are expected to exhibit a notable enrichment in light Cr, which is significantly different from the surface water with very high $\delta^{53}Cr$ values (Qin & Wang, 2017).

Dehydration of serpentinite releases aqueous fluids rich in FMEs and Cr. Previous studies have shown that the interaction with serpentinite-derived fluids led to remarkable Cr enrichment in eclogite from the Western Alps (Angiboust et al., 2014; Spandler et al., 2011). The obviously variable $\delta^{53}Cr$ values of veins imply resolvable Cr isotope fractionation during prograde serpentinite dehydration. These serpentinite-derived fluids with variable $\delta^{53}Cr$ values can interact with subducted slab rocks and modify their Cr isotope composition. On the other hand, as serpentinite is the main host of Cr in subducted slabs, the Cr isotope signature of deserpentinization fluids in arc volcanism should be a more faithful tracer than that of FME (e.g., Li, Sr, and Ba) and their isotopic compositions. However, rare Cr isotope investigations have been conducted on metasomatized mantle wedge peridotites and associated arc lavas. Mantle wedge peridotites that are greatly affected by serpentinite-derived fluids, such as those in the source of lavas from the South Sandwich Arc (Tonarini et al., 2011) and the Lesser Antilles Arc (Cooper et al., 2020), may have different Cr isotope compositions from others that lack serpentinite imprints. This hypothesis needs to be tested in the future based on the Cr isotope systematics of supra-subduction peridotites and worldwide arc lavas.

7. Conclusions

We present here for the first time high-precision Cr isotope compositions for a unique suite of meta-serpentinites that experienced oceanic hydration and subduction-zone dehydration under increasing P–T conditions. The whole sample set has a large $\delta^{53}Cr$ range from −0.45‰ to 0.61‰. The initial mantle-related magmatic processes, as well as the external influx during prograde metamorphism and rock rehydration during exhumation rehydration, had no significant effects on the Cr isotope composition of the subducted serpentinites. Oceanic serpentinization with remarkable Cr loss can lead to residues with higher $\delta^{53}Cr$ values, while samples with Cr >1,800 ppm typically preserve their BSE-like Cr isotope composition. The subducted Atg-serpentinites show lower $\delta^{53}Cr$ values

than both low-grade serpentinite and higher-grade Chl-harzburgite. This is explained by Cr isotope fractionation during prograde dehydration. During the transformation of low-grade serpentinite to Atg-serpentinite, the recrystallization of new magnetite containing less Cr induces the loss of heavy Cr into Cl-rich fluids. In contrast, the antigorite-breakdown reaction would stabilize magnetite that fixed heavy Cr, resulting in the preferential loss of isotopically lighter Cr. No resolvable Cr isotope fractionation occurs during the transition from Chl-harzburgite to Grt-peridotite, which is ascribed to the limited Cr mobility in Cl-poor aqueous fluids. Our study shows that resolvable Cr isotope fractionation could have occurred during serpentinite dehydration in subduction zones. Fluids released from serpentinite may affect the Cr isotope compositions of other metamorphic rocks within subduction zones, as well as of the overlying mantle wedge peridotites and their derived arc magmas.

Conflict of Interest

The authors declare no conflicts of interest relevant to this study.

Data Availability Statement

The compositional data listed in Table 1, and Tables S1 and S2 in Supporting Information S1 are available at https://doi.org/10.5281/zenodo.8041364. Cite as Xiong et al. (2023).

References

Akizawa, N., Tamura, A., Fukushi, K., Yamamoto, J., Mizukami, T., Python, M., & Arai, S. (2016). High-temperature hydrothermal activities around suboceanic Moho: An example from diopsidite and anorthosite in Wadi Fizh, Oman ophiolite. *Lithos*, *263*, 66–87. https://doi.org/10.1016/j.lithos.2016.07.012

Alt, J. C., Garrido, C. J., Shanks, W. C., III, Turchyn, A., Padron-Navarta, J. A., López Sánchez-Vizcaíno, V., et al. (2012). Recycling of water, carbon, and sulfur during subduction of serpentinites: A stable isotope study of Cerro del Almirez, Spain. *Earth and Planetary Science Letters*, *327*, 50–60. https://doi.org/10.1016/j.epsl.2012.01.029

Angiboust, S., Pettke, T., De Hoog, J. C. M., Caron, B., & Oncken, O. (2014). Channelized fluid flow and eclogite-facies metasomatism along the subduction shear zone. *Journal of Petrology*, *55*(5), 883–916. https://doi.org/10.1093/petrology/egu010

Babechuk, M. G., Kleinhanns, I. C., Reitter, E., & Schoenberg, R. (2018). Kinetic stable Cr isotopic fractionation between aqueous Cr(III)-Cl-H_2O complexes at 25°C: Implications for Cr(III) mobility and isotopic variations in modern and ancient natural systems. *Geochimica et Cosmochimica Acta*, *222*, 383–405. https://doi.org/10.1016/j.gca.2017.10.002

Babechuk, M. G., Kleinhanns, I. C., & Schoenberg, R. (2017). Chromium geochemistry of the ca. 1.85 Ga Flin Flon paleosol. *Geobiology*, *15*(1), 30–50. https://doi.org/10.1111/gbi.12203

Bain, D., & Bullen, T. (2005). Chromium isotope fractionation during oxidation of Cr(III) by manganese oxides. *Geochimica et Cosmochimica Acta*, *69*(Supplement), S212.

Berry, A. J., O'Neill, H. S. C., Scott, D. R., Foran, G. J., & Shelley, J. M. G. (2006). The effect of composition on Cr^{2+}/Cr^{3+} in silicate melts. *American Mineralogist*, *91*(11–12), 1901–1908. https://doi.org/10.2138/am.2006.2097

Bodinier, J. L., & Godard, M. (2014). Orogenic, ophiolitic, and abyssal peridotites. In H. D. Holland & K. K. Turekian (Eds.), *Treatise on geochemistry* (2nd ed., pp. 103–167). Elsevier. https://doi.org/10.1016/B978-0-08-095975-7.00204-7

Bonnand, P., Doucelance, R., Boyet, M., Bachèlery, P., Bosq, C., Auclair, D., & Schiano, P. (2020). The influence of igneous processes on the chromium isotopic compositions of Ocean Island basalts. *Earth and Planetary Science Letters*, *532*, 116028. https://doi.org/10.1016/j.epsl.2019.116028

Bonnand, P., Parkinson, I. J., & Anand, M. (2016). Mass dependent fractionation of stable chromium isotopes in mare basalts: Implications for the formation and the differentiation of the Moon. *Geochimica et Cosmochimica Acta*, *175*, 208–221. https://doi.org/10.1016/j.gca.2015.11.041

Bretscher, A., Hermann, J., & Pettke, T. (2018). The influence of oceanic oxidation on serpentinite dehydration during subduction. *Earth and Planetary Science Letters*, *499*, 173–184. https://doi.org/10.1016/j.epsl.2018.07.017

Cannaò, E., Agostini, S., Scambelluri, M., Tonarini, S., & Godard, M. (2015). B, Sr and Pb isotope geochemistry of high-pressure Alpine metaperidotites monitors fluid-mediated element recycling during serpentinite dehydration in subduction mélange (Cima di Gagnone, Swiss Central Alps). *Geochimica et Cosmochimica Acta*, *163*, 80–100. https://doi.org/10.1016/j.gca.2015.04.024

Cooper, G. F., Macpherson, C. G., Blundy, J. D., Maunder, B., Allen, R. W., Goes, S., et al. (2020). Variable water input controls evolution of the Lesser Antilles volcanic arc. *Nature*, *582*(7813), 525–529. https://doi.org/10.1038/s41586-020-2407-5

Crossley, R. J., Evans, K. A., Reddy, S. M., & Lester, G. W. (2017). Redistribution of iron and titanium in high-pressure ultramafic rocks. *Geochemistry, Geophysics, Geosystems*, *18*(11), 3869–3890. https://doi.org/10.1002/2017gc007145

Debret, B., Bolfan-Casanova, N., Padrón-Navarta, J. A., Martin-Hernandez, F., Andreani, M., Garrido, C. J., et al. (2015). Redox state of iron during high-pressure serpentinite dehydration. *Contributions to Mineralogy and Petrology*, *169*(4), 1–18. https://doi.org/10.1007/s00410-015-1130-y

Debret, B., Garrido, C. J., Pons, M.-L., Bouilhol, P., Inglis, E., López Sánchez-Vizcaíno, V., & Williams, H. (2021). Iron and zinc stable isotope evidence for open-system high-pressure dehydration of antigorite serpentinite in subduction zones. *Geochimica et Cosmochimica Acta*, *296*, 210–225. https://doi.org/10.1016/j.gca.2020.12.001

Debret, B., Reekie, C. D. J., Mattielli, N., Beunon, H., Ménez, B., Savov, I., & Williams, H. M. (2020). Redox transfer at subduction zones: Insights from Fe isotopes in the Mariana forearc. *Geochemical Perspectives Letters*, *12*, 46–51. https://doi.org/10.7185/geochemlet.2003

Deschamps, F., Godard, M., Guillot, S., & Hattori, K. (2013). Geochemistry of subduction zone serpentinites: A review. *Lithos*, *178*, 96–127. https://doi.org/10.1016/j.lithos.2013.05.019

Dilissen, N., Hidas, K., Garrido, C. J., Kahl, W.-A., López Sánchez-Vizcaíno, V., & Padrón-Navarta, J. A. (2018). Textural evolution during high-pressure dehydration of serpentinite to peridotite and its relation to stress orientations and kinematics of subducting slabs: Insights from the Almirez ultramafic massif. *Lithos*, *320–321*, 470–489. https://doi.org/10.1016/j.lithos.2018.09.033

Dilissen, N., Hidas, K., Garrido, C. J., López Sánchez-Vizcaíno, V., & Kahl, W.-A. (2021). Morphological transition during prograde olivine growth formed by high-pressure dehydration of antigorite-serpentinite to chlorite-harzburgite in a subduction setting. *Lithos*, *382–383*, 105949. https://doi.org/10.1016/j.lithos.2020.105949

Evans, B. W., Dyar, M. D., & Kuehner, S. M. (2012). Implications of ferrous and ferric iron in antigorite. *American Mineralogist*, *97*(1), 184–196. https://doi.org/10.2138/am.2012.3926

Evans, B. W., & Trommsdorff, V. (1978). Petrogenesis of garnet lherzolite, Cima di Gagnone, Lepontine Alps. *Earth and Planetary Science Letters*, *40*(3), 333–348. https://doi.org/10.1016/0012-821X(78)90158-9

Farkaš, J., Chrastný, V., Novák, M., Čadkova, E., Pašava, J., Chakrabarti, R., et al. (2013). Chromium isotope variations ($\delta^{53/52}$Cr) in mantle-derived sources and their weathering products: Implications for environmental studies and the evolution of $\delta^{53/52}$Cr in the Earth's mantle over geologic time. *Geochimica et Cosmochimica Acta*, *123*, 74–92. https://doi.org/10.1016/j.gca.2013.08.016

Früh-Green, G. L., Scambelluri, M., & Vallis, F. (2004). O–H isotope ratios of high pressure ultramafic rocks: Implications for fluid sources and mobility in the subducted hydrous mantle. *Contributions to Mineralogy and Petrology*, *141*(2), 145–159. https://doi.org/10.1007/s004100000228

Garrido, C. J., López Sánchez-Vizcaíno, V., Gómez-Pugnaire, M. T., Trommsdorff, V., Alard, O., Bodinier, J.-L., & Godard, M. (2005). Enrichment of HFSE in chlorite-harzburgite produced by high-pressure dehydration of antigorite-serpentinite: Implications for subduction magmatism. *Geochemistry, Geophysics, Geosystems*, *6*, Q01J15. https://doi.org/10.1029/2004gc000791

Halama, R., Bebout, G. E., John, T., & Scambelluri, M. (2012). Nitrogen recycling in subducted mantle rocks and implications for the global nitrogen cycle. *International Journal of Earth Sciences*, *103*(7), 2081–2099. https://doi.org/10.1007/s00531-012-0782-3

Harvey, J., Garrido, C. J., Savov, I., Agostini, S., Padrón-Navarta, J. A., Marchesi, C., et al. (2014). [11]B-rich fluids in subduction zones: The role of antigorite dehydration in subducting slabs and boron isotope heterogeneity in the mantle. *Chemical Geology*, *376*(0), 20–30. https://doi.org/10.1016/j.chemgeo.2014.03.015

Haws, A. A., Starr, P. G., Dragovic, B., Scambelluri, M., Belmonte, D., Caddick, M. J., et al. (2021). Meta-rodingite dikes as recorders of subduction zone metamorphism and serpentinite dehydration: Voltri Ophiolite, Italy. *Chemical Geology*, *565*, 120077. https://doi.org/10.1016/j.chemgeo.2021.120077

Hoogerduijn Strating, E. H., Rampone, E., Piccardo, G. B., Drury, M. R., & Vissers, R. L. M. (1993). Subsolidus emplacement of mantle peridotites during incipient oceanic rifting and opening of the Mesozoic Tethys (Voltri Massif, NW Italy). *Journal of Petrology*, *34*(5), 901–927. https://doi.org/10.1093/petrology/34.5.901

Huang, J., Hao, J., Huang, F., & Sverjensky, D. A. (2019). Mobility of chromium in high temperature crustal and upper mantle fluids. *Geochemical Perspectives Letters*, *12*, 1–6. https://doi.org/10.7185/geochemlet.1926

Jabaloy-Sánchez, A., López Sánchez-Vizcaíno, V., Padrón-Navarta, J. A., Hidas, K., Gómez-Pugnaire, M. T., & Garrido, C. J. (2022). Olivine-rich veins in high-pressure serpentinites: A far-field paleo-stress snapshot during subduction. *Journal of Structural Geology*, *163*, 104721. https://doi.org/10.1016/j.jsg.2022.104721

Jerram, M., Bonnand, P., Harvey, J., Ionov, D., & Halliday, A. N. (2022). Stable chromium isotopic variations in peridotite mantle xenoliths: Metasomatism versus partial melting. *Geochimica et Cosmochimica Acta*, *317*, 138–154. https://doi.org/10.1016/j.gca.2021.10.022

Jerram, M., Bonnand, P., Kerr, A. C., Nisbet, E. G., Puchtel, I. S., & Halliday, A. N. (2020). The δ^{53}Cr isotope composition of komatiite flows and implications for the composition of the bulk silicate Earth. *Chemical Geology*, *551*, 119761. https://doi.org/10.1016/j.chemgeo.2020.119761

John, T., Scambelluri, M., Frische, M., Barnes, J. D., & Bach, W. (2011). Dehydration of subducting serpentinite: Implications for halogen mobility in subduction zones and the deep halogen cycle. *Earth and Planetary Science Letters*, *308*(1–2), 65–76. https://doi.org/10.1016/j.epsl.2011.05.038

Kendrick, M. A., Scambelluri, M., Hermann, J., & Padrón-Navarta, J. A. (2018). Halogens and noble gases in serpentinites and secondary peridotites: Implications for seawater subduction and the origin of mantle neon. *Geochimica et Cosmochimica Acta*, *235*, 285–304. https://doi.org/10.1016/j.gca.2018.03.024

Kendrick, M. A., Scambelluri, M., Honda, M., & Phillips, D. (2011). High abundances of noble gas and chlorine delivered to the mantle by serpentinite subduction. *Nature Geoscience*, *4*(11), 807–812. https://doi.org/10.1038/ngeo1270

Klein-Bendavid, O., Pettke, T., & Kessel, R. (2011). Chromium mobility in hydrous fluids at upper mantle conditions. *Lithos*, *125*(1–2), 122–130. https://doi.org/10.1016/j.lithos.2011.02.002

Kraemer, D., Frei, R., Ernst, D. M., Bau, M., & Melchiorre, E. (2021). Serpentinization in the Archean and Early Phanerozoic – Insights from chromium isotope and REY systematics of the Mg Cr hydroxycarbonate stichtite and associated host serpentinites. *Chemical Geology*, *565*, 120055. https://doi.org/10.1016/j.chemgeo.2020.120055

Larsen, K. K., Wielandt, D., Schiller, M., & Bizzarro, M. (2016). Chromatographic speciation of Cr(III)-species, inter-species equilibrium isotope fractionation and improved chemical purification strategies for high-precision isotope analysis. *Journal of Chromatography A*, *1443*, 162–174. https://doi.org/10.1016/j.chroma.2016.03.040

Liang, Y., & Elthon, D. (1990). Evidence from chromium abundances in mantle rocks for extraction of picrite and komatiite melts. *Nature*, *343*(6258), 551–553. https://doi.org/10.1038/343551a0

López Sánchez-Vizcaíno, V., Trommsdorff, V., Gómez-Pugnaire, M. T., Garrido, C. J., Müntener, O., & Connolly, J. A. D. (2005). Petrology of titanian clinohumite and olivine at the high-pressure breakdown of antigorite serpentinite to chlorite harzburgite (Almirez Massif, S. Spain). *Contributions to Mineralogy and Petrology*, *149*(6), 627–646. https://doi.org/10.1007/s00410-005-0678-3

Ma, H., Xu, L.-J., Shen, J., Liu, S.-A., & Li, S. (2022). Chromium isotope fractionation during magmatic processes: Evidence from mid-ocean ridge basalts. *Geochimica et Cosmochimica Acta*, *327*, 79–95. https://doi.org/10.1016/j.gca.2022.04.018

Marchesi, C., Garrido, C. J., Padrón-Navarta, J. A., López Sánchez-Vizcaíno, V., & Gómez-Pugnaire, M. T. (2013). Element mobility from seafloor serpentinization to high-pressure dehydration of antigorite in subducted serpentinite: Insights from the Cerro del Almirez ultramafic massif (southern Spain). *Lithos*, *178*, 128–142. https://doi.org/10.1016/j.lithos.2012.11.025

Marshall, D., Groat, L., Giuliani, G., Murphy, D., Mattey, D., Ercit, T. S., et al. (2003). Pressure, temperature and fluid conditions during emerald precipitation, southeastern Yukon, Canada: Fluid inclusion and stable isotope evidence. *Chemical Geology*, *194*(1–3), 187–199. https://doi.org/10.1016/S0009-2541(02)00277-2

McClain, C. N., & Maher, K. (2016). Chromium fluxes and speciation in ultramafic catchments and global rivers. *Chemical Geology*, *426*, 135–157. https://doi.org/10.1016/j.chemgeo.2016.01.021

McDonough, W. F., & Sun, S. S. (1995). The composition of the Earth. *Chemical Geology*, *120*(3–4), 223–253. https://doi.org/10.1016/0009-2541(94)00140-4

Menzel, M. D., Garrido, C. J., & López Sánchez-Vizcaíno, V. (2020). Fluid-mediated carbon release from serpentinite-hosted carbonates during dehydration of antigorite-serpentinite in subduction zones. *Earth and Planetary Science Letters*, *531*, 115964. https://doi.org/10.1016/j.epsl.2019.115964

Menzel, M. D., Garrido, C. J., López Sánchez-Vizcaíno, V., Hidas, K., & Marchesi, C. (2019). Subduction metamorphism of serpentinite-hosted carbonates beyond antigorite-serpentinite dehydration (Nevado-Filábride Complex, Spain). *Journal of Metamorphic Geology*, *37*(5), 681–715. https://doi.org/10.1111/jmg.12481

Montanini, A. (2006). Exhumation history of a garnet pyroxenite-bearing mantle section from a continent-ocean transition (Northern Apennine Ophiolites, Italy). *Journal of Petrology*, *47*(10), 1943–1971. https://doi.org/10.1093/petrology/egl032

Nimis, P., & Trommsdorff, V. (2001). Revised thermobarometry of Alpe Arami and other garnet peridotites from the Central Alps. *Journal of Petrology*, *42*(1), 103–115. https://doi.org/10.1093/petrology/42.1.103

Niu, Y. (2004). Bulk-rock major and trace element compositions of abyssal peridotites: Implications for mantle melting, melt extraction and post-melting processes beneath mid-ocean ridges. *Journal of Petrology*, *45*(12), 2423–2458. https://doi.org/10.1093/petrology/egh068

Novak, M., Andronikov, A. V., Sebek, O., Kotkova, J., Erban Kochergina, Y. V., Stepanova, M., et al. (2022). Chromium isotope systematics in three mantle-derived domains of Central European Variscides: Relationship between δ^{53}Cr values and progressive weathering of serpentinized ultramafic rocks. *Chemical Geology*, *604*, 120940. https://doi.org/10.1016/j.chemgeo.2022.120940

Novak, M., Kram, P., Sebek, O., Andronikov, A., Chrastny, V., Martinkova, E., et al. (2017). Temporal changes in Cr fluxes and δ53Cr values in runoff from a small serpentinite catchment (Slavkov Forest, Czech Republic). *Chemical Geology*, *472*, 22–30. https://doi.org/10.1016/j.chemgeo.2017.09.023

O'Neill, H. S. C., & Berry, A. J. (2021). The oxidation state of chromium in basaltic silicate melts. *Geochimica et Cosmochimica Acta*, *306*, 304–320. https://doi.org/10.1016/j.gca.2021.03.024

Oze, C., Sleep, N. H., Coleman, R. G., & Fendorf, S. (2016). Anoxic oxidation of chromium. *Geology*, *44*(7), 543–546. https://doi.org/10.1130/G37844.1

Padrón-Navarta, J. A., Hermann, J., Garrido, C. J., López Sánchez-Vizcaíno, V., & Gómez-Pugnaire, M. T. (2010). An experimental investigation of antigorite dehydration in natural silica-enriched serpentinite. *Contributions to Mineralogy and Petrology*, *159*(1), 25–42. https://doi.org/10.1007/s00410-009-0414-5

Padrón-Navarta, J. A., López Sánchez-Vizcaíno, V., Garrido, C. J., & Gomez-Pugnaire, M. T. (2011). Metamorphic record of high-pressure dehydration of antigorite serpentinite to chlorite harzburgite in a subduction setting (Cerro del Almirez, Nevado-Filabride Complex, Southern Spain). *Journal of Petrology*, *52*(10), 2047–2078. https://doi.org/10.1093/petrology/egr039

Padrón-Navarta, J. A., López Sánchez-Vizcaíno, V., Hermann, J., Connolly, J. A. D., Garrido, C. J., Gómez-Pugnaire, M. T., & Marchesi, C. (2013). Tschermak's substitution in antigorite and consequences for phase relations and water liberation in high-grade serpentinites. *Lithos*, *178*, 186–196. https://doi.org/10.1016/j.lithos.2013.02.001

Padrón-Navarta, J. A., López Sánchez-Vizcaíno, V., Menzel, M. D., Gómez-Pugnaire, M. T., & Garrido, C. J. (2023). Mantle wedge oxidation from deserpentinization modulated by sediment-derived fluids. *Nature Geosciences*, *16*(3), 268–275. https://doi.org/10.1038/s41561-023-01127-0

Padrón-Navarta, J. A., Tommasi, A., Garrido, C. J., & Mainprice, D. (2015). On topotaxy and compaction during antigorite and chlorite dehydration: An experimental and natural study. *Contributions to Mineralogy and Petrology*, *169*(4), 1–20. https://doi.org/10.1007/s00410-015-1129-4

Penniston-Dorland, S. C., Kohn, M. J., & Manning, C. E. (2015). The global range of subduction zone thermal structures from exhumed blueschists and eclogites: Rocks are hotter than models. *Earth and Planetary Science Letters*, *428*, 243–254. https://doi.org/10.1016/j.epsl.2015.07.031

Pettke, T., & Bretscher, A. (2022). Fluid-mediated element cycling in subducted oceanic lithosphere: The orogenic serpentinite perspective. *Earth-Science Reviews*, *225*, 103896. https://doi.org/10.1016/j.earscirev.2021.103896

Piccoli, F., Hermann, J., Pettke, T., Connolly, J. A. D., Kempf, E. D., & Vieira, D. J. F. (2019). Subducting serpentinites release reduced, not oxidized, aqueous fluids. *Scientific Reports*, *9*(1), 19573. https://doi.org/10.1038/s41598-019-55944-8

Ping, X., Wang, X., Zheng, J., Liu, Y., Su, Y., Chen, H., et al. (2022). The stable chromium isotope composition of different mantle reservoirs. *Geochimica et Cosmochimica Acta*, *338*, 24–33. https://doi.org/10.1016/j.gca.2022.09.025

Plank, T. (2014). The chemical composition of subducting sediments. In H. D. Holland & K. K. Turekian (Eds.), *Treatise on geochemistry* (2nd ed., pp. 607–629). Elsevier. https://doi.org/10.1016/B978-0-08-095975-7.00319-3

Pons, M. L., Debret, B., Bouilhol, P., Delacour, A., & Williams, H. (2016). Zinc isotope evidence for sulfate-rich fluid transfer across subduction zones. *Nature Communications*, *7*(1), 13794. https://doi.org/10.1038/ncomms13794

Qin, L. P., & Wang, X. L. (2017). Chromium isotope geochemistry. *Reviews in Mineralogy and Geochemistry*, *82*(1), 379–414. https://doi.org/10.2138/rmg.2017.82.10

Roeder, P. L., & Reynolds, I. (1991). Crystallization of chromite and chromium solubility in basaltic melts. *Journal of Petrology*, *32*(5), 909–934. https://doi.org/10.1093/petrology/32.5.909

Saad, E. M., Wang, X., Planavsky, N. J., Reinhard, C. T., & Tang, Y. (2017). Redox-independent chromium isotope fractionation induced by ligand-promoted dissolution. *Nature Communications*, *8*(1), 1590. https://doi.org/10.1038/s41467-017-01694-y

Scambelluri, M., Cannaò, E., & Gilio, M. (2019). The water and fluid-mobile element cycles during serpentinite subduction. A review. *European Journal of Mineralogy*, *31*(3), 405–428. https://doi.org/10.1127/ejm/2019/0031-2842

Scambelluri, M., Müntener, O., Ottolini, L., Pettke, T. T., & Vannucci, R. (2004). The fate of B, Cl and Li in the subducted oceanic mantle and in the antigorite breakdown fluids. *Earth and Planetary Science Letters*, *222*(1), 217–234. https://doi.org/10.1016/j.epsl.2004.02.012

Scambelluri, M., Pettke, T., & Cannaò, E. (2015). Fluid-related inclusions in Alpine high-pressure peridotite reveal trace element recycling during subduction-zone dehydration of serpentinized mantle (Cima di Gagnone, Swiss Alps). *Earth and Planetary Science Letters*, *429*, 45–59. https://doi.org/10.1016/j.epsl.2015.07.060

Scambelluri, M., Pettke, T., Rampone, E., Godard, M., & Reusser, E. (2014). Petrology and trace element budgets of high-pressure peridotites indicate subduction dehydration of serpentinized mantle (Cima di Gagnone, Central Alps, Switzerland). *Journal of Petrology*, *55*(3), 459–498. https://doi.org/10.1093/petrology/egt068

Scambelluri, M., Piccardo, G. B., Philippot, P., Robbiano, A., & Negretti, L. (1997). High salinity fluid inclusions formed from recycled seawater in deeply subducted alpine serpentinite. *Earth and Planetary Science Letters*, *148*(3–4), 485–499. https://doi.org/10.1016/S0012-821X(97)00043-5

Scambelluri, M., Rampone, E., & Piccardo, G. B. (2001). Fluid and element cycling in subducted serpentinite: A trace-element study of the Erro–Tobbio high-pressure ultramafites (Western Alps, NW Italy). *Journal of Petrology*, *42*(1), 55–67. https://doi.org/10.1093/petrology/42.1.55

Scambelluri, M., & Tonarini, S. (2012). Boron isotope evidence for shallow fluid transfer across subduction zones by serpentinized mantle. *Geology*, *40*(10), 907–910. https://doi.org/10.1130/g33233.1

Schauble, E., Rossman, G. R., & Taylor, H. P. (2004). Theoretical estimates of equilibrium chromium-isotope fractionations. *Chemical Geology*, *205*(1–2), 99–114. https://doi.org/10.1016/j.chemgeo.2003.12.015

Schoenberg, R., Zink, S., Staubwasser, M., & von Blanckenburg, F. (2008). The stable Cr isotope inventory of solid Earth reservoirs determined by double spike MC-ICP-MS. *Chemical Geology*, *249*(3–4), 294–306. https://doi.org/10.1016/j.chemgeo.2008.01.009

Shen, J., Liu, J., Qin, L., Wang, S.-J., Li, S., Xia, J., et al. (2015). Chromium isotope signature during continental crust subduction recorded in metamorphic rocks. *Geochemistry, Geophysics, Geosystems*, *16*(11), 3840–3854. https://doi.org/10.1002/2015gc005944

Shen, J., Qin, L., Fang, Z., Zhang, Y., Liu, J., Liu, W., et al. (2018). High-temperature intermineral Cr isotope fractionation: A comparison of ionic model predictions and experimental investigations of mantle xenoliths from the North China Craton. *Earth and Planetary Science Letters*, *499*, 278–290. https://doi.org/10.1016/j.epsl.2018.07.041

Shen, J., Wang, S.-J., Qin, L., Ni, H., Li, S., Du, J., et al. (2021). Tracing serpentinite dehydration in a subduction channel: Chromium element and isotope evidence from subducted oceanic crust. *Geochimica et Cosmochimica Acta*, *313*, 1–20. https://doi.org/10.1016/j.gca.2021.06.030

Shen, J., Xia, J., Qin, L., Carlson, R. W., Huang, S., Helz, R. T., & Mock, T. D. (2020). Stable chromium isotope fractionation during magmatic differentiation: Insights from Hawaiian basalts and implications for planetary redox conditions. *Geochimica et Cosmochimica Acta*, *278*, 289–304. https://doi.org/10.1016/j.gca.2019.10.003

Spandler, C., Pettke, T., & Rubatto, D. (2011). Internal and external fluid sources for eclogite-facies veins in the Monviso meta-ophiolite, Western Alps: Implications for fluid flow in subduction zones. *Journal of Petrology*, *52*(6), 1207–1236. https://doi.org/10.1093/petrology/egr025

Spandler, C., & Pirard, C. (2013). Element recycling from subducting slabs to arc crust: A review. *Lithos*, *170–171*, 208–223. https://doi.org/10.1016/j.lithos.2013.02.016

Syracuse, E. M., van Keken, P. E., & Abers, G. A. (2010). The global range of subduction zone thermal models. *Physics of the Earth and Planetary Interiors*, *183*(1–2), 73–90. https://doi.org/10.1016/j.pepi.2010.02.004

Tonarini, S., Leeman, W. P., & Leat, P. T. (2011). Subduction erosion of forearc mantle wedge implicated in the genesis of the South Sandwich Island (SSI) arc: Evidence from boron isotope systematics. *Earth and Planetary Science Letters*, *301*(1–2), 275–284. https://doi.org/10.1016/j.epsl.2010.11.008

Trommsdorff, V., López Sánchez-Vizcaíno, V., Gómez-Pugnaire, M. T., & Müntener, O. (1998). High pressure breakdown of antigorite to spinifex-textured olivine and orthopyroxene, SE Spain. *Contributions to Mineralogy and Petrology*, *132*(2), 139–148. https://doi.org/10.1007/s004100050412

Vieira Duarte, J. F., Piccoli, F., Pettke, T., & Hermann, J. (2021). Textural and geochemical evidence for magnetite production upon antigorite breakdown during subduction. *Journal of Petrology*, *62*(10), egab053. https://doi.org/10.1093/petrology/egab053

Wagner, L. J., Kleinhanns, I. C., Weber, N., Babechuk, M. G., Hofmann, A., & Schoenberg, R. (2021). Coupled stable chromium and iron isotopic fractionation tracing magmatic mineral crystallization in Archean komatiite-tholeiite suites. *Chemical Geology*, *576*, 120121. https://doi.org/10.1016/j.chemgeo.2021.120121

Wang, X. L., Johnson, T. M., & Ellis, A. S. (2015). Equilibrium isotopic fractionation and isotopic exchange kinetics between Cr(III) and Cr(VI). *Geochimica et Cosmochimica Acta*, *153*, 72–90. https://doi.org/10.1016/10.1016/j.gca.2015.01.003

Wang, X. L., Planavsky, N. J., Reinhard, C. T., Zou, H., Ague, J. J., Wu, Y., et al. (2016). Chromium isotope fractionation during subduction-related metamorphism, black shale weathering, and hydrothermal alteration. *Chemical Geology*, *423*, 19–33. https://doi.org/10.1016/j.chemgeo.2016.01.003

Watenphul, A., Schmidt, C., & Jahn, S. (2014). Cr(III) solubility in aqueous fluids at high pressures and temperatures. *Geochimica et Cosmochimica Acta*, *126*, 212–227. https://doi.org/10.1016/j.gca.2013.10.054

White, W. M., & Klein, E. M. (2014). Composition of the oceanic crust. In H. D. Holland & K. K. Turekian (Eds.), *Treatise on geochemistry* (2nd ed., pp. 457–496). Elsevier. https://doi.org/10.1016/B978-0-08-095975-7.00315-6

Whitney, D. L., & Evans, B. W. (2010). Abbreviations for names of rock-forming minerals. *American Mineralogist*, *95*(1), 185–187. https://doi.org/10.2138/am.2010.3371

Xia, J. X., Qin, L. P., Shen, J., Carlson, R. W., Ionov, D. A., & Mock, T. D. (2017). Chromium isotope heterogeneity in the mantle. *Earth and Planetary Science Letters*, *464*, 103–115. https://doi.org/10.1016/j.epsl.2017.01.045

Xiong, J.-W., Chen, Y.-X., Shen, J., Marchesi, C., Scambelluri, M., Qin, L.-P., et al. (2023). Compositional data for "Chromium isotope behavior during serpentinite dehydration in oceanic subduction zones" [Dataset]. Zenodo. https://doi.org/10.5281/zenodo.8041364

Zhang, Q., Liu, J., Zhang, Y., Yu, H., Qin, L., & Shen, J. (2019). Factors affecting chromium isotope measurements using the double-spike method. *Rapid Communications in Mass Spectrometry*, *33*, 1390–1400. https://doi.org/10.1002/rcm.8483

Zhang, Y. X., Gazel, E., Gaetani, G. A., & Klein, F. (2021). Serpentinite-derived slab fluids control the oxidation state of the subarc mantle. *Science Advances*, *7*(48), eabj2515. https://doi.org/10.1126/sciadv.abj2515

Zink, S., Schoenberg, R., & Staubwasser, M. (2010). Isotopic fractionation and reaction kinetics between Cr(III) and Cr(VI) in aqueous media. *Geochimica et Cosmochimica Acta*, *74*(20), 5729–5745. https://doi.org/10.1016/j.gca.2010.07.015

References From the Supporting Information

Jochum, K. P., Weis, U., Schwager, B., Stoll, B., Wilson, S. A., Haug, G. H., et al. (2016). Reference values following ISO guidelines for frequently requested rock reference materials. *Geostandards & Geoanalytical Research*, *40*(3), 333–350. https://doi.org/10.1111/j.1751-908X.2015.00392.x